University of Texas at El Paso
ScholarWorks@UTEP

Open Access Theses & Dissertations

2023-12-01

Using Shallow Electromagnetic and Magnetic Techniques to Map Soil Texture and Characterize Salinity and Water Dynamics Below Pecan Orchards, El Paso County, Texas

Kristina Sasser
University of Texas at El Paso

Follow this and additional works at: https://scholarworks.utep.edu/open_etd

 Part of the Geophysics and Seismology Commons

Recommended Citation

Sasser, Kristina, "Using Shallow Electromagnetic and Magnetic Techniques to Map Soil Texture and Characterize Salinity and Water Dynamics Below Pecan Orchards, El Paso County, Texas" (2023). *Open Access Theses & Dissertations*. 4019.
https://scholarworks.utep.edu/open_etd/4019

This is brought to you for free and open access by ScholarWorks@UTEP. It has been accepted for inclusion in Open Access Theses & Dissertations by an authorized administrator of ScholarWorks@UTEP. For more information, please contact lweber@utep.edu.

USING SHALLOW ELECTROMAGNETIC AND MAGNETIC TECHNIQUES TO MAP SOIL TEXTURE AND CHARACTERIZE SALINITY AND WATER DYNAMICS BELOW PECAN ORCHARDS, EL PASO COUNTY, TEXAS

KRISTINA LYNN SASSER

Master's Program in Geophysics

APPROVED:

Mark Engle, Ph.D., Chair

Lixin Jin, Ph.D.

Anthony Darrouzet-Nardi, Ph.D.

Diane Doser, Ph.D.

Stephen L. Crites, Jr., Ph.D.
Dean of the Graduate School

Copyright ©

by

Kristina Lynn Sasser

2023

USING SHALLOW ELECTROMAGNETIC AND MAGNETIC TECHNIQUES TO MAP SOIL TEXTURE AND CHARACTERIZE SALINITY AND WATER DYNAMICS BELOW PECAN ORCHARDS, EL PASO COUNTY, TEXAS

by

KRISTINA LYNN SASSER, B.S.

THESIS

Presented to the Faculty of the Graduate School of

The University of Texas at El Paso

in Partial Fulfillment

of the Requirements

for the Degree of

MASTER OF SCIENCE

Department of Earth, Environmental and Resource Sciences

THE UNIVERSITY OF TEXAS AT EL PASO

December 2023

Acknowledgements

The successful completion of this thesis research has been a collective effort, and I am immensely grateful for the individuals and organizations who have been instrumental over the past two years. Foremost among them is my advisor, Dr. Mark Engle, whose great mentorship, and profound knowledge have guided my academic growth. I would also like to thank Mark Baker who created the inversion program I utilized in my research and for help at various steps along the way. My committee members, Dr. Lixin Jin, Dr. Diane Doser, and Dr. Anthony Darrouzet-Nardi have provided me with integral feedback that greatly contributed to the robustness of this work. I would also like to acknowledge the help I received from Frida Garcia Ledezma, who processed soil texture data, as well as Jessica Hartman, Aracely Garcia, and Christian Leach for their assistance in collecting field data. Thank you to Galen Kaip for his training in the use of electromagnetics and magnetics instruments, a skillset that proved to be vital to this research. I am thankful for the Ivey family and staff at 5R Pecan Orchard for permitting me to conduct this research on their properties. Financial support for this research was made possible through the U.S. National Science Foundation grant #2012475 and #2034312. Lastly, I want to extend my heartfelt appreciation to my family, boyfriend, and friends who have provided me with unwavering support throughout my academic journey.

Abstract

Non-invasive, near surface geophysical tools provide a time efficient and cost-effective approach to study the shallow subsurface. Electromagnetic induction (EMI) instruments are a category of these near surface methods that provide spatial and temporal information (2-D to 4-D) about shallow (<6 m) subsurface properties, from which soil salinity, clay content, and water content can be estimated. However, deconstructing soil apparent electrical conductivity (EC_a) from EMI methods into its component parts remains a challenge.

This research uses EMI and magnetic geophysical techniques to: (1) compare and contrast the distribution and behavior of EC_a, both spatially and temporally, at two flood irrigated agricultural sites (pecan orchards) with different soil layers, properties, and controls on electrical conductivities that lie within the same floodplain in far west Texas; and (2) develop a one-dimensional inversion model using EC_a and soil texture data at specified layers from established sites of known high and low EC_a to determine soil layer resistivities at various dates during the irrigation season. Data are compared to soil sensor bulk EC and volumetric water content data at corresponding depths to validate results.

Soils at both sites exhibit large EC_a contributions from textural controls, and irrigation frequency. The combination of these two controls dictate where and how quickly secondary minerals precipitate, clog soil pores, reduce infiltration, and salinize the groundwater. Insight from this research aids in ongoing efforts to characterize vadose zone hydrology in dryland critical zones with high infiltration and serves as a guide for locations where future soil sampling will occur.

Table of Contents

List of Tables

List of Figures

Section 1: Introduction

Since the 1970s, electromagnetic induction (EMI) instruments have been used in agricultural fields to quantify subsurface apparent electrical conductivity (EC_a [mS/m]) in the upper few meters of soil (de Jong et al., 1979; Doolittle & Brevik, 2014). From the resulting measurements, soil characteristics such as texture, clay content, soil salinity, depth to water table, and soil water content can be inferred (De Carlo et al., 2021; Wollenhaupt et al., 1986; Zhao et al., 2011). For example, Altdorff et al. (2020) used EMI instruments in a corn field to determine a positive correlation ($p<0.05$) from EC_a to silt and soil water content under dry conditions, relatively stable correlations of EC_a to sand, silt, and soil water content under wet conditions, and negative correlations of EC_a to sand in dry conditions. However, these soil characteristics vary spatially and temporally in agricultural fields, and thus EC_a measurements and corresponding interpretations typically require site-specific validation by soil collection and analyses along a transect or excavated pits (De Carlo et al., 2021). Physical and geochemical methods have been individually used at pedon scales to determine soil characteristics but have limited functionality and coverage across large areas such as entire agricultural sites, which generally cover the hectare scale. Therefore, the combination of EMI with point physical and geochemical measurements have the ability to validate soil parameters and infer spatial and temporal variations across agricultural sites.

EMI instruments have also successfully been used in regional investigations to map the distribution of soil properties in natural and developed sites along the Rio Grande flood plain in far west Texas and south-central New Mexico (Doser & Baker, 2021). Soils along this floodplain are developed on alluvial sediments and are heterogeneous in both their layering and texture, due to the ancestral Rio Grande's variation in flow and channel location (Doser et al., 2019). The variability in soil properties is apparent across very small horizontal distances (<10 m). The

research presented in this thesis focuses on two neighboring (~2.5 km apart) flood irrigated pecan orchards (5R and Ivey) in Tornillo, Texas (Figure 1). Leveraging successful application of EMI instruments and other shallow geophysical methods in both agricultural fields and along the Rio Grande, I hypothesized that these approaches allow for an understanding of the subsurface at these sites. 5R and Ivey are a part of The Dryland Critical Zone Thematic Cluster, a National Science Foundation funded study, which concentrates on investigating critical zone science at dryland sites, across a gradient of climate and land use.

In this research, EMI and magnetic susceptibility methods were used to monitor and compare the spatial and temporal distribution of soil layer EC_a at and between 5R and Ivey pecan orchards. Repeated EC_a measurements, taken over time at select periods between flood irrigation events, were used to correlate EC_a data with temporal capacitive soil sensor data to provide a near real-time means for tracking soil layer EC_a, particle size, salt, and water content. However, parsing soil EC_a into its component parts remains a complex challenge. A linear unmixing model was applied to determine individual EC_a contributions from individual layers with time. Using external sources of texture, soil moisture and porewater EC data, an attempt was made to parse soil layer EC_a into particle size, salt, and water components at both sites. Efforts were made to link these results together when geochemical data are unavailable, serving as a foundation for informed agricultural decision-making. Outcomes from this research will assist the Dryland Critical Zone Project's effort to characterize shallow subsurface processes and hydrology at sites with high infiltration.

Section 2: Background

2.1 Pecan Orchard Sites

This investigation focuses on the characterization and data collection of soil properties from 5R and Ivey pecan orchards located in Tornillo Texas, ~65 km southeast of the University of Texas at El Paso (UTEP). Both sites sit within the Upper Rio Grande valley (Figure 1), which is one of many extensional basins that together form the Rio Grande Rift system (Mack & Leeder, 1998). The Hueco Bolson aquifer lies beneath the region, spanning ~2,150 km² and measures an average of ~2,745 m deep. Borehole electric-log interpretations from nearby (~12 km away) Fabens, Texas suggest that the deepest parts of the Hueco Bolson are composed of thick sedimentary sequences deposited during the Paleogene (Figure 2) (Hawley et al., 2009). During the Pliocene and Early Pleistocene, large volumes of sediments were delivered to the southeastern Hueco Bolson surface via the ancestral Rio Grande and are now covered by fluvial sediments extending up to 30 km across and 300 m thick (Figure 3). The bulk of these sediments are ephemeral-lake deposits of the Fort Hancock (mid- to upper Santa Fe Group, >2.5 Ma,) and Camp Rice (upper Santa Fe Group, <2.5 Ma) (Figure 4) (Hawley et al., 2009). The entrenched river-valley system in the Fabens area has a floodplain elevation ~1,100 m, with a 300 m wide river-valley floor composed of bedrock from Lower Cenozoic sandstones, mudstones, conglomerates with minor or no volcanic constituents, and sedimentary rocks (Hawley et al., 2009). The inner-valley alluvial fill channel and floodplain deposits, which underlie the two pecan orchards being studied as part of this investigation, are less than 30 m saturated thickness and consist of mostly pebble to cobble gravel, gravel, sand, silt, and clay.

2.2 SOILS

In the early 1900s, the Rio Grande floor in south-central New Mexico and far west Texas frequently migrated and avulsed across the valley, leading to parent material deposits and present-day soils (Mack & Leeder, 1998; Doser et al., 2019). At the 5R study site, the National Resources Conservation Service (2021) categorizes the soil as Harkey loam (Ha) and Harkey silty clay loam (Hk) (Figure 5). These relatively young soils are derived from Rio Grande-related proximal levee and proximal crevasse splay deposits of the Holocene age (Doser et al., 2019). A hand-augered borehole within a subsection of 5R indicates soil texture consisting of loam to a depth of 0.38 m, silty fine sand from 0.38 to 0.94 m, silty clay from 0.94 to 1.09 m, loam from 1.09 to 1.47 m, silty clay from 1.47 to 1.75 m, loam from 1.75 to 2.39 m, clay from 2.39 to 2.72 m, and fine, saturated sand from 2.72 to 2.89 m (Liu & Sheng, 2013).

The National Resources Conservation Service (2021) categorizes the soil at Ivey to be comprised of Gila fine sandy loam (Ga), Glendale silty clay loam (Ge), Harkey loam (Ha), Harkey silty clay loam (Hk), Saneli silty clay loam (Sa) and Tigua silty clay (Tg) (Figure 6). Ga and Ge are formed from distal crevasse splays; Ha and Hk from proximal levee/crevasse splays; and Sa and Tg from floodplain derived soils (Doser et al., 2019). Between 100-150 cm depth, the soil texture at the Pecan_fine_Ivey site is silty clayey, while the Pecan_coarse_Ivey site is sandy; with both sites exhibiting coarser textures at deeper depths (Ortiz, 2018). The soil electrical conductivity values at the Pecan_fine_Ivey site are higher than those at the Pecan_coarse_Ivey site; with both sites exhibiting peak values between 100-150 cm depth. Immediately following flood irrigation at 15 cm depth, the Pecan_fine_Ivey site exhibits twice the soil moisture content as the Pecan_coarse_Ivey site (Ortiz, 2018).

2.3 Previous Geophysical Surveys

Previous EMI surveys were conducted at Ivey across a 100 m^2 area (Figure 5), but the EM31 (deeper measurements) and EM38 data (shallower measurements) have an eight-year gap, and the EM38 data exhibited unusually high EC_a values ranging from 40-240 mS/m (Garcia, 2021). A 100 m long resistivity survey conducted at Ivey in April 2018 (Sosa, 2019; Garcia, 2021) produced a 2-dimensional inverted conductivity model of the unsaturated subsurface where finely textured areas (Pecan_fine_Ivey) had EC_a values between 155–402 mS/m, and coarser textured areas (Pecan_coarse_Ivey) had EC_a values between 60-130 mS/m (Sosa, 2019). These measurements correlate with soil texture, tree growth, and tree size. At Ivey, Sosa (2019) conducted a seismic survey in April 2018 and determined the depth to the static water table is ~2 m and fluctuates ~1.1-2.2 m below ground surface, following one irrigation event.

2.4 Irrigation Practices

Both agricultural sites are subject to seasonal flood irrigation, consisting of an annual total of 1.5 m of water distributed in aliquots every two to three weeks from April to October, which significantly dominates the mean annual precipitation of ~16-25 cm the region receives (Table 1) (Ortiz et al., 2022). During wet or normal flow years for the upper Rio Grande, irrigation water is obtained from the river, containing total dissolved solids (TDS) values of 500-1,500 mg/L (Doser et al., 2019; Ortiz et al., 2022). However, since 2000 the upper Rio Grande has largely been in a drought condition (Sheng & Liu, 2015) which has forced growers to obtain irrigation water from nearby shallow brackish groundwater containing 2,000-3,000 mg/L TDS (Miyamoto et al., 1995). Evapotranspiration between irrigation events, limited water infiltration, and the practice of flood irrigating with water containing high TDS values over multiple growing seasons leads to salt accumulation and altered crop health (Ortiz & Jin, 2021, Ortiz et al., 2022). Salt buildup and

evaporation are accelerated due to these salts clogging soil pores, and decreasing salt leaching (Ortiz & Jin, 2021). While sandy soils can exhibit high permeability and can drain highly saline irrigation water, clay soils often do not drain well potentially leading to high salinity which can result in salt accumulation and crop damage (Miyamoto et al., 1995).

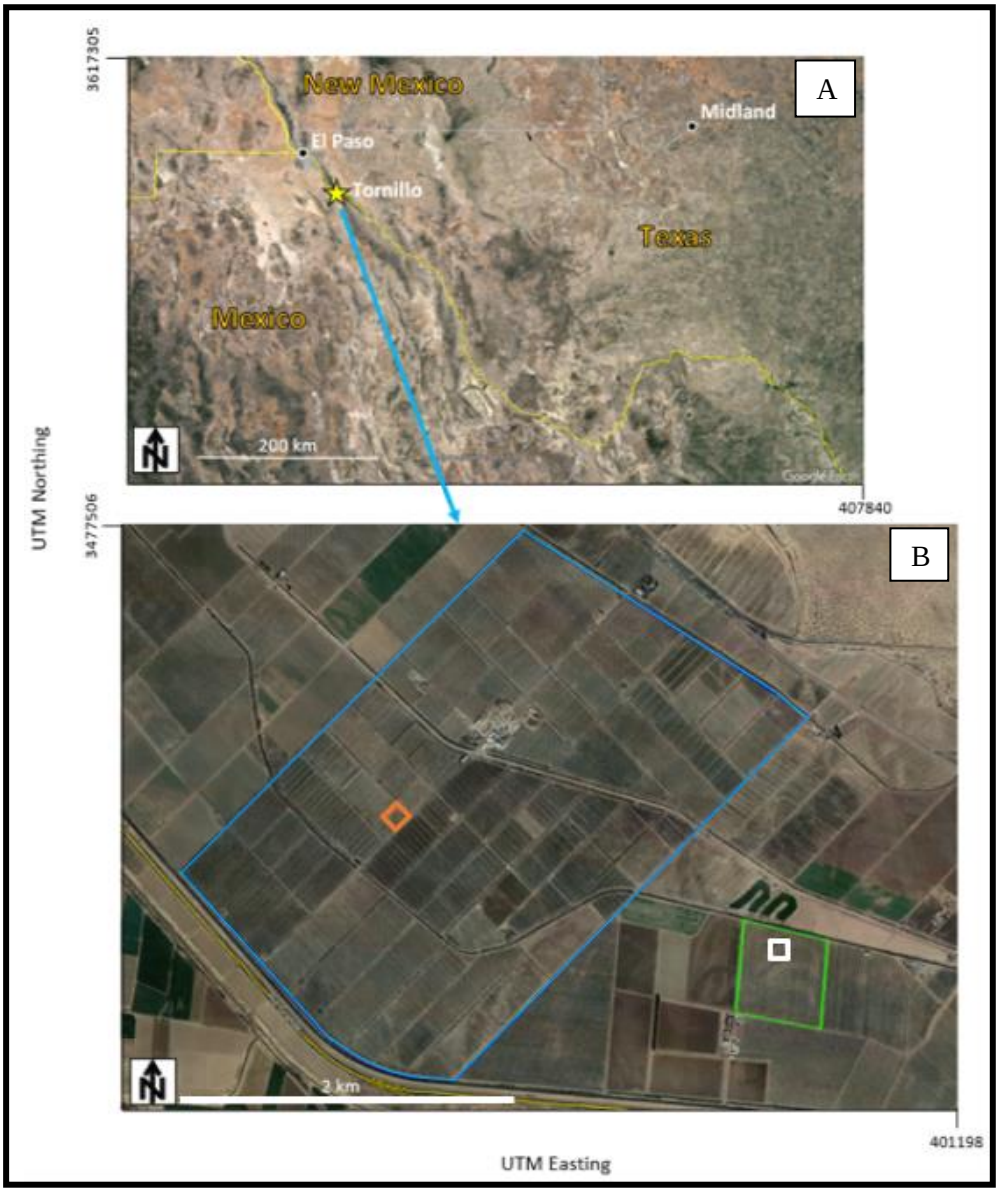

Figure 1: (A) A map of southwest Texas, northern Mexico, and southern New Mexico. Study sites are located in Tornillo, Texas, north of the Rio Grande. (B) A map of 5R Pecan Orchard (blue), the 5R study area (orange), Ivey Pecan Orchard (green) and the Ivey study area (white).

<table>
<tr><th>Age (Years)</th><th>Epoch</th><th colspan="4">Hydrostratigraphic Units (HSU)</th></tr>
<tr><td>0 – 100,000</td><td>Holocene
Upper Pleistocene</td><td colspan="4">Rio Grande Deposits
Valley-border Alluvium
Basin Floor Units</td></tr>
<tr><td rowspan="2">100,000 – 750,000</td><td rowspan="2">Middle Pleistocene</td><td colspan="4">Basin-Fill Facies Assemblages</td></tr>
<tr><td colspan="2">Basin Floor</td><td colspan="2">Piedmont Slope</td></tr>
<tr><td>750,000 – 10 Ma</td><td>Lower Pleistocene
Pliocene
Upper Miocene</td><td rowspan="3">Santa Fe Group</td><td>Upper Santa Fe (USF2, 4)</td><td rowspan="3">Undivided Facies Assemblages (LSF, MSF,USF)</td><td>Upper Santa Fe (USF1, 3, 5)</td></tr>
<tr><td>10 Ma – 16.5 Ma</td><td>Middle Miocene</td><td>Middle Santa Fe (MSF2)</td><td>Middle Santa Fe (MSF1, 3, 5)</td></tr>
<tr><td>16.5 – 22 Ma</td><td>Lower Miocene</td><td>Lower Santa Fe (LSF2)</td><td>Lower Santa Fe (LSF1, 3)</td></tr>
<tr><td>22 Ma – 42 Ma</td><td>Oligocene
Eocene</td><td colspan="4">Unclassified Bedrock Units</td></tr>
</table>

Figure 2 (adapted from Hawley et al., 2009): Correlation between major chronologic, and hydrostratigraphic units that make up the Paso del Norte region, south-central New Mexico, western Trans-Pecos Texas, and adjacent parts of Chihuahua, Mexico. Hydrostratigraphic units are mappable basin- and valley-fill sequence deposits grouped via position in chronostratigraphic contexts.

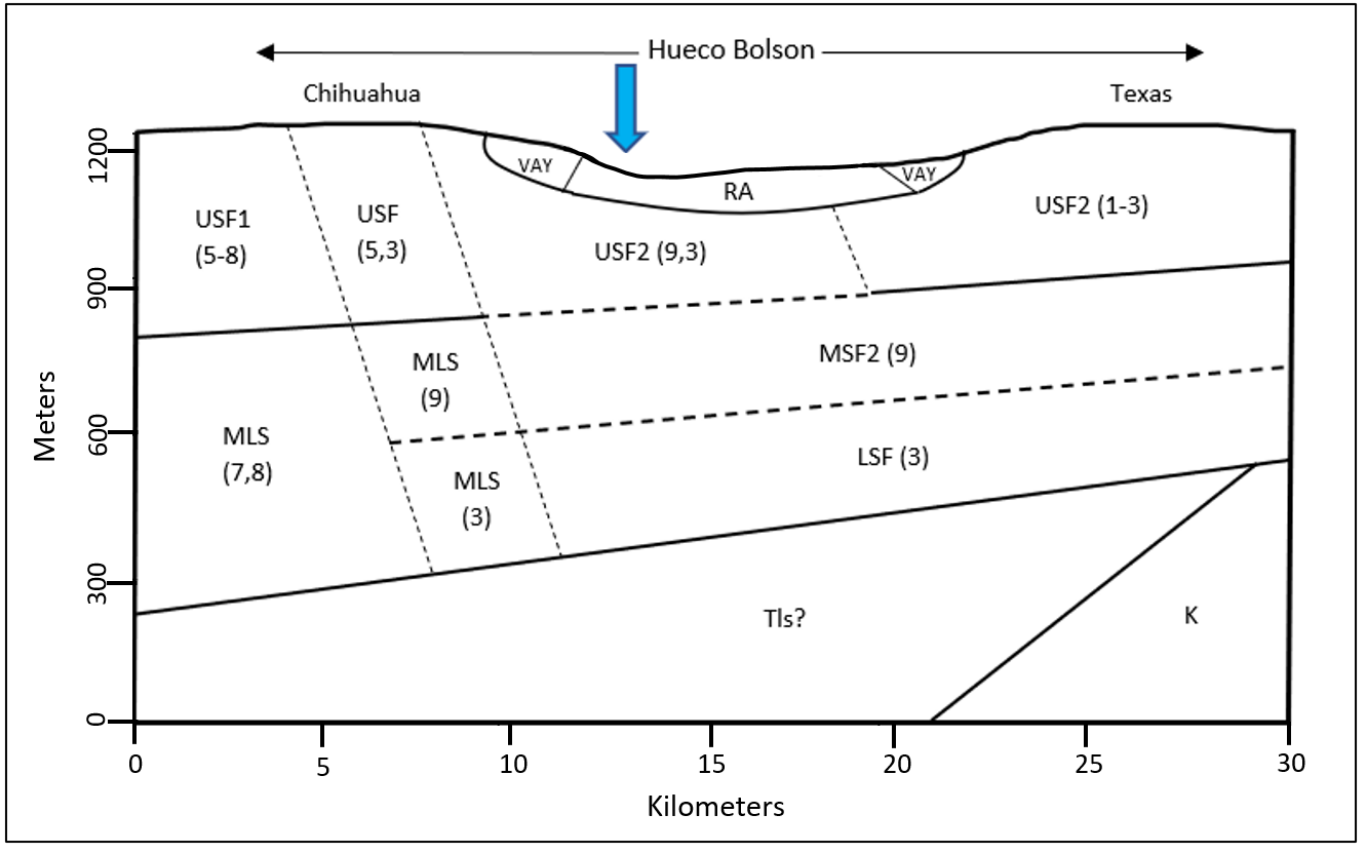

Figure 3 (adapted from Hawley et al., 2009): A cross-section index map of the Hueco Bolson, showing locations of schematic hydrogeologic sections. The blue arrow indicates the United States/Mexico boundary and Rio Grande river in Fabens, Texas. Rio Grande Alluvium (RA) - River-channel and floodplain deposits of the Rio Grande; up to 30 m saturated thickness; upper shallow aquifer zone. Upper Santa Fe HSUs (USF2)- Basin-floor facies; includes Camp Rice Formation subdivisions; up to 3 m of upper Quaternary eolian cover is locally present; Early to Late Miocene. Middle Santa Fe HSUs (MSF2)- Basin-floor facies undivided; primarily weakly to moderately indurated pebbly sandstones, sandstones, and mudstones mostly in the zone of saturation; includes Rincon Valley Fm correlatives. Lower Santa Fe HSUs (LSF)- Undivided piedmont and basin-floor facies; fanglomerate, conglomerate, conglomeratic sandstone, siltstone, and mudstone with thin, limestone and gypsum layers; Upper Cenozoic-Miocene.

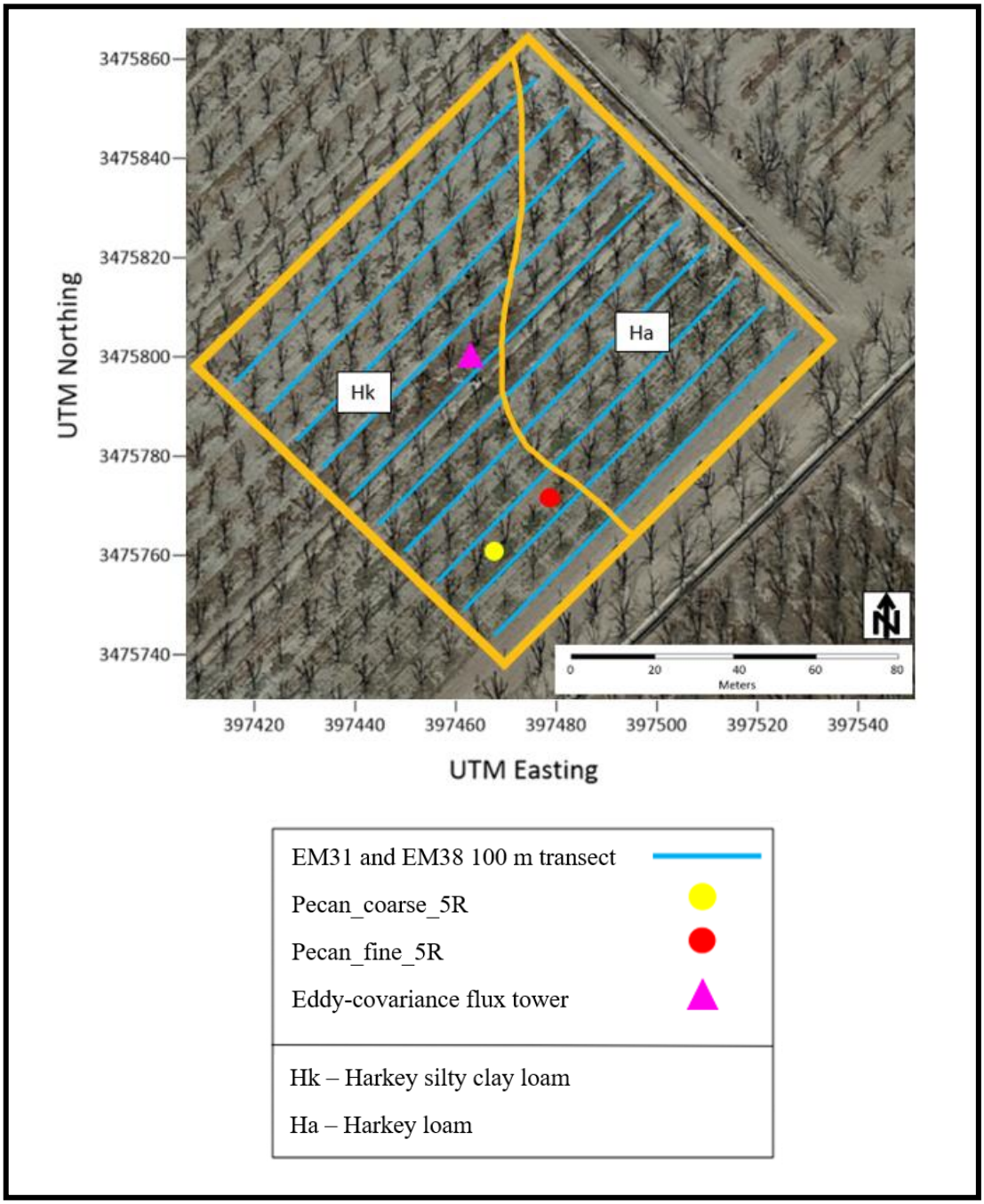

Figure 4: A 2021 soils map of the area of interest at 5R pecan orchard in Tornillo, Texas. The Rio Grande is approximately 1,200 m southwest of the site. The blue lines represent 100 m EMI survey lines taken in 2022. The yellow and red dots represent locations of boreholes where soil volumetric water content, grain size, electrical conductivity, CO_2 and O_2 sensors are located were installed in July 2022. The fuchsia triangle represents the Eddy-covariance flux tower.

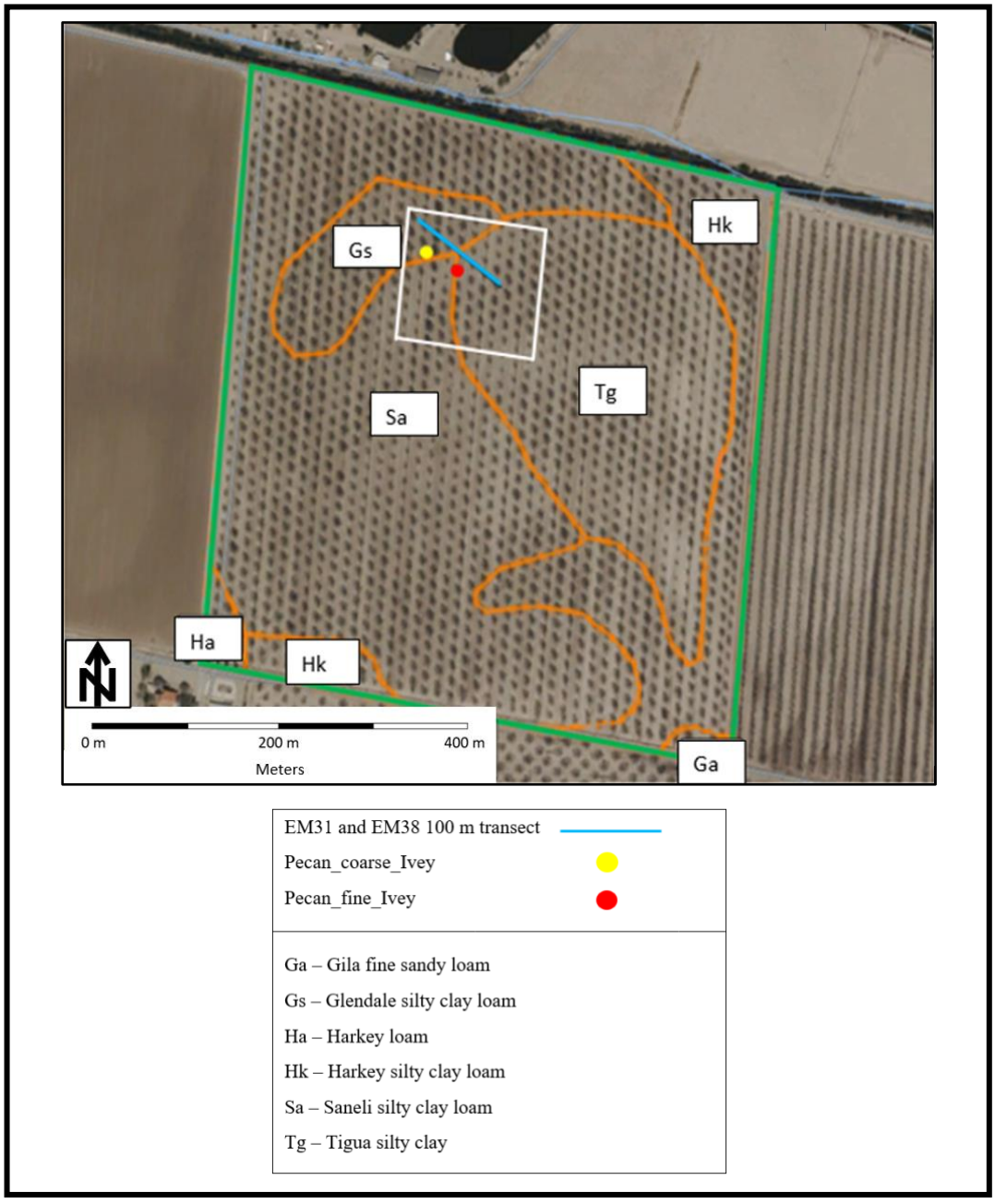

Figure 5: A 2021 soils map of Ivey pecan orchard in Tornillo, Texas. The green area is the entire orchard, and small white area is the area of interest. The Rio Grande is approximately 600 m south of the site. The blue line represents a 100 m transect where EMI time series surveys were recorded during and post-irrigation season in 2022. The yellow and red dots represent locations of boreholes where soil volumetric water content, grain size, electrical conductivity, CO_2 and O_2 sensors are located.

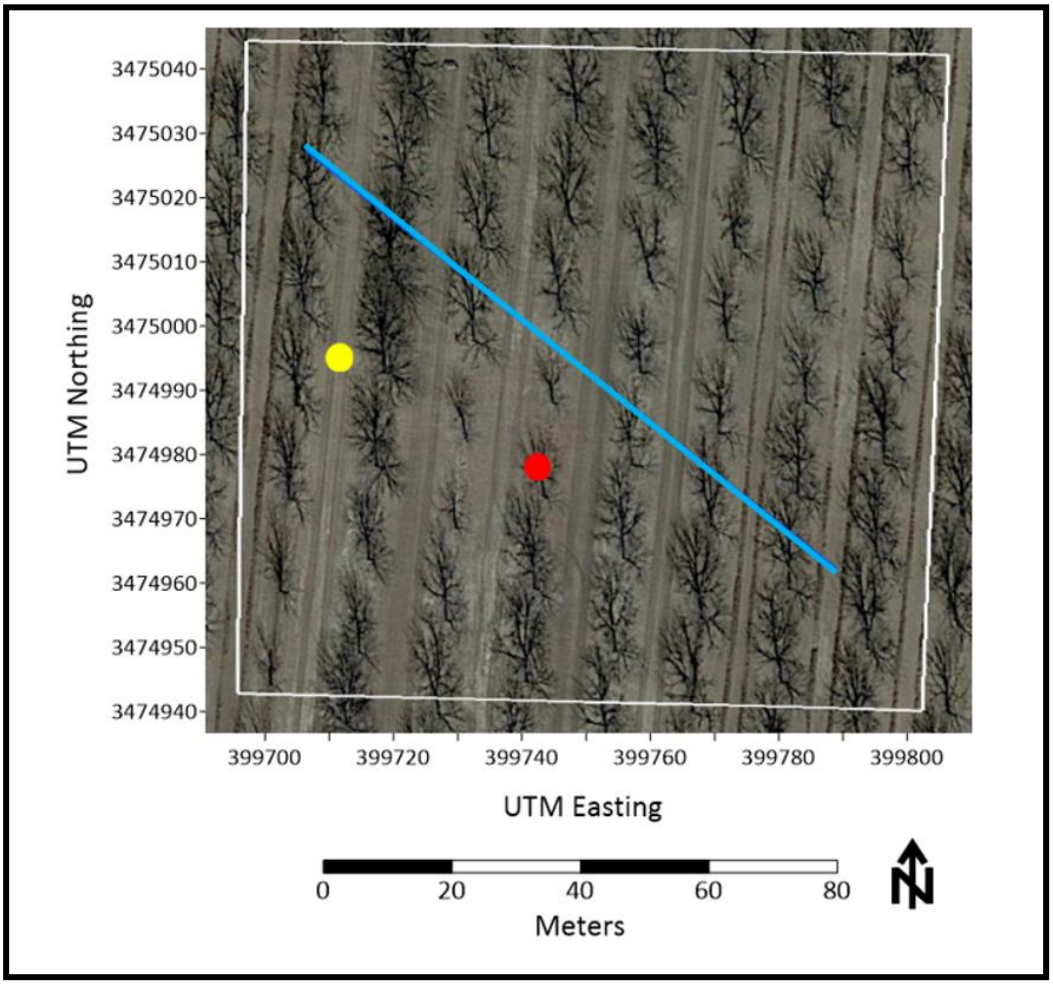

Figure 6: A map of the area of interest at Ivey pecan orchard. The blue line represents a 100 m transect where EMI measurements were repeated beginning in the northwest and ending in the southeast during and after the 2022 irrigation season.

Table 1: Irrigation schedules and water source for (A) 5R in 2023 and (B) Ivey in 2022.

A

5R Pecan Orchard	
Irrigation Date	**Water Source**
3/3/2023	Groundwater
5/10/2023	River Water
5/30/2023	River Water
6/22/2023	River Water
7/12/2023	River Water
7/30/2023	River Water
8/18/2023	River Water
9/13/2023	River Water

B

Ivey Pecan Orchard	
Irrigation Date	**Water Source**
4/23/2022	Unknown
5/20/2022	Unknown
6/13/2022	River Water
7/9/2022	River Water
7/28/2022	River Water
8/17/2022	River Water
9/17/2022	Groundwater

Section 3: Methods

3.1 Electromagnetic Induction

EMI sensors quantify the magnitude of soil EC_a and apparent magnetic susceptibility (MS_a) of a sampled volume of earthen materials. In these instruments, a transmitter coil generates an alternating current that extends into the subsurface creating an electromagnetic field, known as the primary field. Electrically conductive materials in the subsurface create eddy currents in response to the field created from the transmitter coil, and a corresponding secondary electromagnetic field is produced. The receiver coil records the signal as a sum of the primary and secondary fields (Figure 7). By design, a bucking coil removes the signal of the primary field at the receiver, resulting in a recording dominated by the secondary magnetic field: a function of the operating frequency, ground conductivity, and intercoil spacing (McNeill, 1980).

The principle of Faraday's Law governs the operation of EMI instruments (Eq. 1) where the electromotive force (EMF) recorded in the receiver is the sum of the EMF generated by the transmitter and that induced by subsurface conductors:

$$EMF_R = M_{RT}\frac{dI_T}{dt} + M_{RC}\frac{dI_C}{dt}, \qquad \text{Eq. 1}$$

where EMF_R is the electromotive force (voltage) in the receiver, M_{RT} is the mutual inductance between the receiver (*R*) and transmitter (*T*), M_{RC} is the mutual inductance (a complex number) between the receiver (*R*) and conductor (*C*) in the ground, $\frac{dI_C}{dt}$ or $\frac{dI_T}{dt}$ are the time derivatives of the current induced in the conductor (*C*) or transmitter (*T*), and I_T or I_C is the current induced in the conductor (*C*) or transmitter (*T*). The secondary field comprises the quadrature phase component, 90 degrees out of phase with the primary transmitted field and directly linked to subsurface conductivity, and the in-phase component, completely in phase with the primary transmitted field and directly associated with magnetic susceptibility (Geonics Limited, 2016; De Carlo et al., 2021).

The depth-weighted EC_a measurements are determined via comparing field strength in the transmitting and receiving coils (Robinet et al., 2018) and have a direct relationship with soil water content, clay content, salinity, texture, and temperature (Doolittle & Brevik, 2014; Doser et al., 2019). When administered over time, EMI surveys allow for documenting EC_a changes to further determine where the greatest subsurface heterogeneities lie, and how the relationship of flood irrigation events alter EC_a (Doser et al., 2004).

For EMI measurement, the Geonics Limited EM31-MK2 (herein referred to as the EM31) and EM38-MK2 (herein referred to as the EM38) were used at the pecan orchards to measure EC_a values. Each instrument has a horizonal dipole orientation (HDO) and a vertical dipole orientation (VDO) in which the orientation of the instrument during data collection dictates the nominal depth of produced EC_a values. The EM31 has a 3.66 m spacing between the transmitting and receiving coil, providing a nominal depth of investigation (DOI) of ~3 and ~6 m when operated in the HDO and VDO, respectively. The EM38 has two receiver coils that are separated from the transmitter coil at 1.0 and 0.5 m, resulting in a DOI of ~1.5 and ~0.75 m in VDO and ~0.75 and ~0.375 m in HDO (Figure 8) (Doolittle & Brevik, 2014; Pathirana et al., 2023). The EC_a values are depth integrated (cumulative response of a multi-layered earth) in a non-linear manner and extend beyond the nominal DOI (McNeill, 1980) (Figure 9). That is, with the EM38 in VDO, the cumulative contribution from all ground elements below a depth of 0.4 meters is ~78%, whereas in HDO, the cumulative contribution from all ground elements below the same depth is ~49%.

Time series EMI data were collected at both sites, as described in the following sections, to (1) to track the effects of irrigation water on soil water content and salinity; (2) investigate the contributions of soil texture, water content and salinity toward EC_a; and (3) examine EC_a as a function of depth at the various DOIs at different points in time.

3.1.1 5R Pecan Orchard

A baseline EMI survey was conducted at 5R in March 2022 prior to the initiation of flood irrigation season to aid in soil characterization, identification of controls on water movement in the vadose zone and to allow for comparison of interpretations between the two sites. While this same sequence of data collection previously occurred at Ivey (Garcia, 2021), the application of this methodology to 5R furthers soil property interpretation and comparison between the two sites. The survey consisted of ten 100 m lines, with data points collected in vertical and horizontal orientations every 1 m (Figure 4) taking a total of two days to complete. The EM31 and EM38 were calibrated at the start of each day. The EM38 was subsequently recalibrated every 1.5-2 hours, while the EM31 was recalibrated every 5-6 hours, according to manufacturer recommendations. Repeat measurements were collected at the first point of each line after completing that line in order to assess instrument calibration drift during the run. No systematic shifts were observed. Golden Software's Surfer 23 program was used to contour EC_a data collected at nominal depths of 0.375, 0.75, 1.5, 3.0, and 6.0 m using a minimum curvature interpolation algorithm (Figures 10A-10F). To perform the interpolation at each depth, the grid geometry was set to the bounds of the GPS coordinates (100 nodes in each direction). The maximum residual limit of 0.18 was imposed, the anisotropy ratio was set to 1 (i.e., isotropic), and a total of 100,000 iterations were conducted. Data beyond the alpha shape value of 11.222 were restricted, and a linear Z-transform was configured.

Time series EMI surveys were conducted using both the EM31 and EM38 in vertical and horizontal orientations before and during the 2023 crop irrigation season along a northeast-southwest trending 100 m transect between tree lines across the Pecan_fine_5R and Pecan_coarse_5R borehole locations. These surveys were conducted for two purposes: (1)

periodically from February to September to identify low-frequency and seasonal trends throughout non-irrigation and irrigation seasons, and (2) every other day after a single irrigation event from September 2-12, 2023 to track high-frequency variations in the EC_a response to one irrigation event.

3.1.2 Ivey Pecan Orchard

Throughout the 2022 crop irrigation season, time series EMI surveys using both the EM31 and EM38 in vertical and horizontal orientations were conducted at Ivey monthly and every other day following a single irrigation event in July 2022 along the same 100 m transect as the 2-D resistivity survey of Sosa (2019) to track temporal EC_a changes. Monthly surveys involved data collection seven to nineteen days after each irrigation event and ran from June until October when the soil dried out substantially. High frequency surveys began in July approximately six days following an irrigation event and continued until the following irrigation cycle began for a robust look into EC_a changes at different depths throughout one entire irrigation cycle.

3.1.2.1 1-Dimensional Inversion

Inversion of the conductivity data were attempted using a bespoke software package (Integrated Resistivity, version 2.1.1.2) made available by Dr. Mark Baker. The program uses a least-norm a priori approach to generate expected equations of non-zero layer conductivities determined from the multi-height EM38 conductivity measurements (or more generally any electrical conductivity or resistivity data) through shifting the equation system's origin to that of the theoretical layer conductivity. A function for a continuous random variable is in turn generated via comparing exact solutions to a related problem with expected layer conductivities, resulting in an analytic approach to solving a problem that exhibits nonuniqueness.

At Ivey, EM38 data were collected on 9/6/2023 at Pecan_coarse_Ivey and Pecan_fine_Ivey sites in order to calibrate a constrained inversion model using the program. EC_a data from these locations were collected at heights of 0.0, 0.5, and 1.0 m above the ground in VDO and HDO. These data were used as model inputs in the Integrated Resistivity software alongside simultaneously recorded soil sensor bulk EC data converted into resistivity.

At Pecan_fine_Ivey, the layer structure was divided into seven layers above a half-space (Table 2A). The top layer accounts for space between the instrument and the ground (air, grass, tree litter, roots), followed by five layers of 0.30 m in thickness which correlate to and span the depth of all five soil sensors (0.30, 0.60, 0.90, 1.2, and 1.5 m). A 2.0 m layer lies above the half-space which accounts for the area beneath the soil sensors and above the groundwater table. The inversion was performed to constrain the resistivities of the top, bottom, and half-space layers ensuring that they were consistent with the EMI data. The resulting soil layer resistivities were then converted into EC and compared to soil bulk EC and volumetric water content (VWC) data at corresponding depths and times of EC_a data collection (Figure 18A).

While the same layer structure used to model Pecan_coarse_Ivey was attempted to divide soil layers at Pecan_fine_Ivey, the resulting model produced resistivity values that trended in the opposite direction as corresponding soil sensor data. Instead, Pecan_coarse_Ivey soil layers and thicknesses were determined from soil texture and soil sensor bulk EC data collected by Ortiz & Jin (2021) (Table 2B) and used as inputs into the program. The uppermost layer was modeled to be 0.36 m thick, reported to consist of relatively equal weights of sand and silt (39-50%) with little clay (6-11%). The second layer was modeled to be 0.60 m thick and was composed of >50% sand by weight. From ~1.0-1.5 m, the soil layer was characterized by relatively finer, yet still sandy material. At this depth range, the highest columnar bulk EC values were exhibited (0.47-2.48

dS/m) (Ortiz & Jin, 2021). The fourth layer was modeled to be 0.97 m thick, ranging between 91-97% clay by weight, and contained the lowest columnar soil bulk EC (0.33-0.66 dS/m). The inversion was performed to constrain the resistivity of each layer, from which each were converted into EC and compared to soil bulk EC and VWC data at corresponding depths and times (Figure 18C).

The model layer architecture produced by the multi-height data collected on 9/6/2023 at both sites were applied to EC_a data collected along the 100 m transect at 0 m above the ground on 7/16/2022 near the Pecan_fine_Ivey and Pecan_coarse_Ivey sites. These EC_a data were used as program inputs to determine soil layer resistivities on this date. Individual soil layer resistivities were converted to EC and compared to soil sensor bulk EC and VWC at corresponding depths and plotted as a function of depth (Figures 18B and 18D).

3.2 MAGNETIC SUSCEPTIBILITY

Magnetic susceptibility is a measure of the ability for a material to take on an induced magnetism due to its presence in the Earth's magnetic field. Magnetometers measure the small scalar magnitude variations in Earth's magnetic field on a nanotesla level which allows for quantification of subsurface magnetic content and differentiation between materials of varying iron contents (specifically hematite and magnetite), grain sizes, buried metal objects, and major soil units (Doser et al., 2019). The Geometrics G857 proton-precession magnetometer, which was used in this investigation, contains a sensor enclosed by a hydrogen-rich fluid (i.e., kerosene in this case), surrounded by a coil of wire, energized by a direct current to produce a strong magnetic field, forcing all protons to align in a certain direction, resulting in a MS_a reading. Drift corrections are necessary in magnetic surveys as Earth's magnetic field is in constant flux with the sun, and Earth's convecting molten outer core is continuously moving. Diurnally, as the sun approaches zenith,

magnetic field values increase, after which they decrease until sunset. Events such as thunderstorms and solar storms can create large spikes in magnetic field readings, impacting processing methods. Additionally, magnetic anomalies such as metal barrels and pipes can cause data distortion. To resolve this, data were reduced to the pole (RTP), which converts a magnetic anomaly created by an arbitrary source into an anomaly that the same source would create if it was located at the pole and is magnetized solely by induction (Luo et al., 2010).

3.2.1 5R Pecan Orchard

In April 2022, a magnetic survey was conducted at 5R over the same ten 100 m lines as the March 2022 EMI survey (Figure 4), but with data points collected once every two meters instead of every meter. Before and after each line of data collection, base station measurements were taken to later correct for drift. The survey area's ambient magnetic field, inclination, and declination were calculated at the time of the survey using the National Geophysical Data Center's Magnetic field calculator (World Magnetic Model 2019-2024). The ambient magnetic field was 46,647.9 nT, the declination was 7.5026 degrees east, and the inclination was 58.7329 degrees. Relative to the ambient magnetic field, the observed MS_a data exhibited fluctuations of approximately ±400 nT; which signified a magnetic anomaly was present. Subsequently, it was eliminated via an RTP calculation: for each station (reference point), a 20 m vertical line element magnetic dipole was placed with its top situated 10 m below the measured elevation. Then, the magnetic declination and inclination were used to conduct a simultaneous equation solution to estimate the magnetic moment within the dipole. The effects of 80, 120, and 200 m radius cutoffs were explored to refine the solution. The 80 m radius cutoff was utilized as it provided sufficient smoothing when coupled with interpolation. The magnetic anomaly was then recalculated with a 90 degree inclination and a 0 degree declination. Magnetic anomaly data that exceeded ±10 nT from the ambient magnetic

field were excluded from further processing. Golden Software's Surfer 23 program was used to contour the RTP MS_a data using a minimum curvature interpolation algorithm (Figure 10F). To conduct the interpolation, the grid geometry was established based on the GPS coordinates (100 nodes in each direction). A maximum residual limit of 0.60 was applied, the anisotropy ratio was set to 1, and 100,000 iterations were performed. Data outside the bounds of the alpha shape value of 14.088 were restricted, and a linear Z-transform was applied.

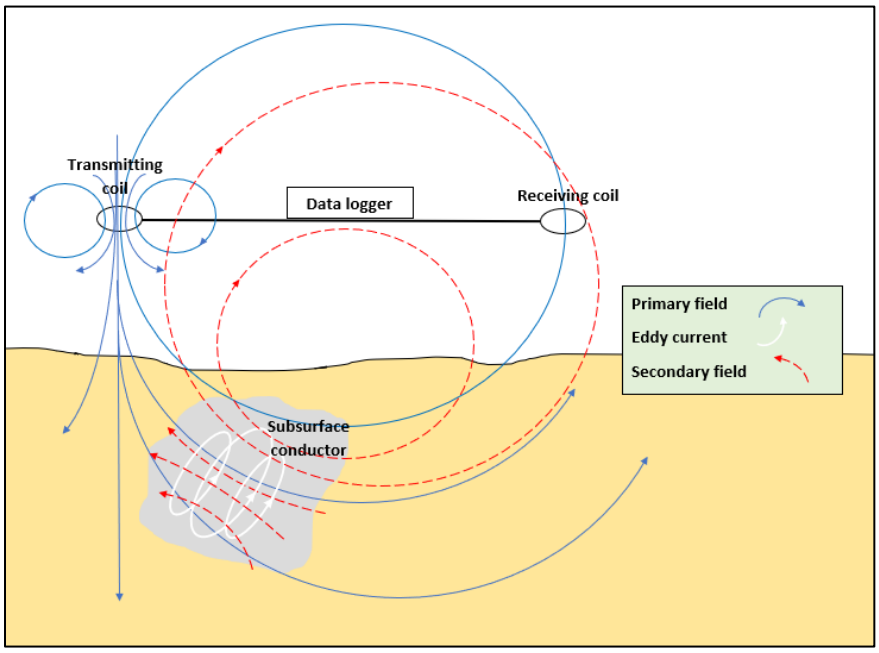

Figure 7 (adapted from De Carlo et al., 2022): A cartoon illustrating the function of EMI instruments.

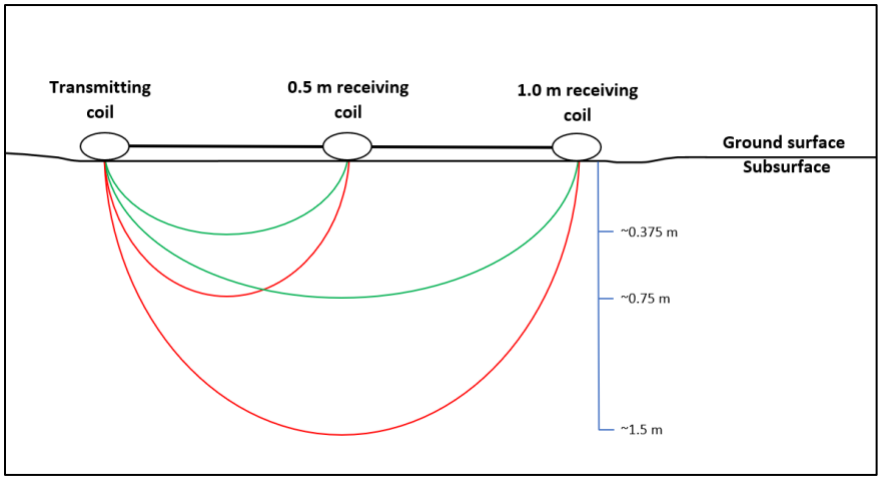

Figure 8 (adapted from Pathirana et al., 2023): A diagram depicting the EM38's approximate sampled volume of earthen material and corresponding approximate depths of investigation. As the coil spacing increases, the DOI increases. The green curves approximate the bounded volume of earth sampled in HDO, while the red curves approximate the bounded volume of earth sampled in VDO.

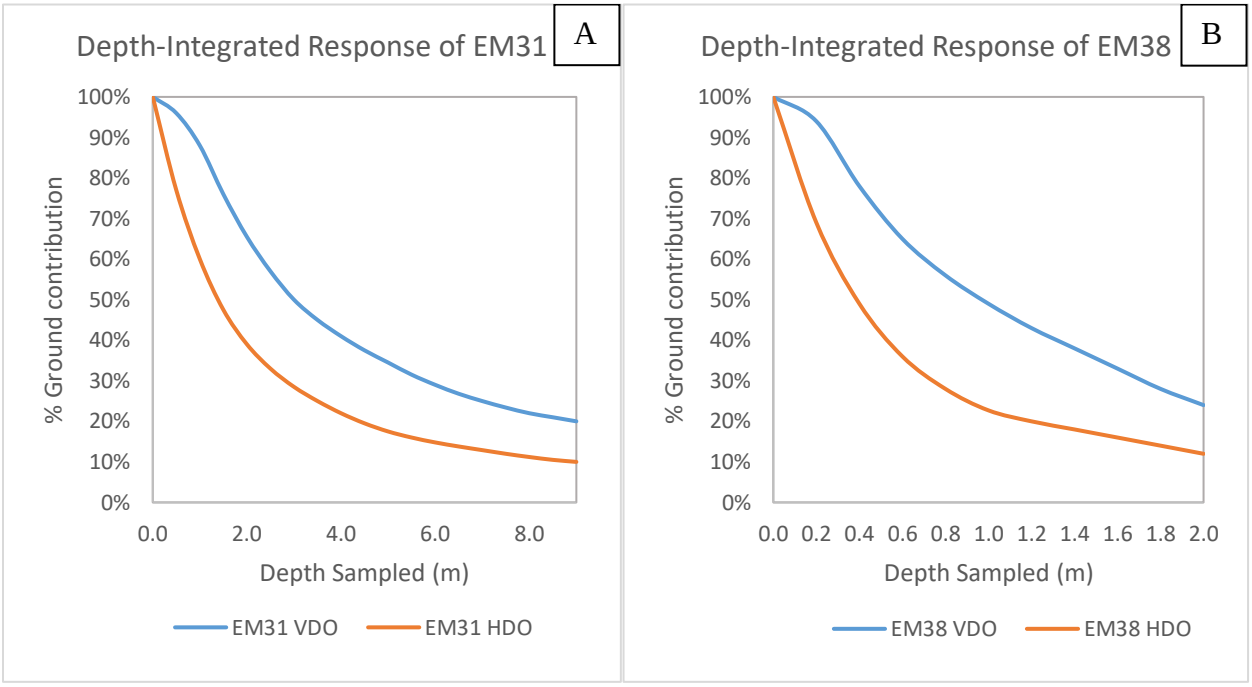

Figure 9 (adapted from Geonics Limited, 2007; Geonics Limited 2016): The approximate cumulative depth-integrated response of a multi-layered earth for (A) the EM31 and (B) the EM38 when both instruments are placed on the ground.

Table 2: Ivey soil layer thicknesses and total depth to the bottom of the corresponding layer at (A) Pecan_fine_Ivey and (B) Pecan_coarse_Ivey used in modeled soil EC.

A

Pecan_fine_Ivey	
Layer Thickness (m)	Depth (m)
0.15	0.15
0.30	0.45
0.30	0.75
0.30	1.05
0.30	1.35
0.30	1.65
2.00	3.65
H-S	10

B

Pecan_coarse_Ivey	
Layer Thickness (m)	Depth (m)
0.36	0.36
0.60	0.96
0.50	1.46
0.97	2.43
H-S	10

Section 4: Results

4.1 5R Pecan Orchard

4.1.1 Electromagnetic Induction Surveys

Baseline survey results from March 2022 show that EC_a values increase as a function of depth (Figures 10A-10E). From depths of 0.375 to 3.0 m, vertically persistent low EC_a zones trend north to south and in the eastern corner of the EMI survey area (20-120 mS/m and 20-140 mS/m, respectively), while vertically persistent high EC_a zones border the northwest and southeast edges of the maps (140-220 mS/m and 140-260 mS/m, respectively) (Figures 10A-10D). At 6.0 m, high EC_a ranging from 220-260 mS/m were identified in a zone trending west to southeast (Figure 10E). Based on this survey, sites of high EC_a (Pecan_fine_5R) and low EC_a (Pecan_coarse_5R) were identified (Figure 4). In July 2022, vertical soil samples were collected down to 3.0 m depth, and Campbell Scientific TEROS 12 soil sensors were installed at depths of 0.3, 0.6, 0.9, 1.2, and 1.5 m to monitor soil bulk EC and VWC. Additionally, EOSense EosGP sensors were installed to monitor CO_2 at 0.3 and 0.6 m depths, and Apogee SO-110 sensors were installed to monitor O_2 at 0.3 and 0.6 m depths.

Monthly EMI surveys along the 100 m transect show temporal variations in the EC_a (Figures 11A-11E). The highest EC_a across all DOI occurred on 9/28/2023, after the eighth irrigation event of the season (which occurred 15 days prior). On this date, the highest EC_a responses occurred at 6.0 m and ranged from 126.5 to 263.25 mS/m, with the peak EC_a response occurring at 65 m (~4 m away from Pecan_fine_5R) (Figure 11E). Conversely, the lowest EC_a responses across all DOI were recorded early in the irrigation season on 4/16/2023 and 5/9/2023 (44 and 67 days after the first, and most recent irrigation occurred, respectively) (Figures 11A-11E). These low EC_a responses occurred between 92 and 94 m (4-6 m away from

Pecan_coarse_5R) and increased as DOI increased (7.55 mS/m at 0.375 m; 25.22 mS/m at 0.75 m; 47.14 mS/m at 1.5 m; 85.75 mS/m at 3.0 m; and 126.50 mS/m at 6.0 m, respectively). Across all DOI, the date with the least amount of variation in EC_a responses occurs on 2/17/2023, two weeks prior to the initial irrigation event.

Data collected on 5/9/2023 and 9/2/2023 were normalized to data from 2/17/2023 to show linear shifts in EC_a from this baseline (Figures 13A-13E). Data collected on 5/9/2023 (67 days after the first and most recent irrigation) show baseline EC_a shifts that are small, and often negative (Figures 13A-13E). The largest positive shifts in EC_a responses along the transect occur late in the irrigation season on 9/2/2023 (after the seventh irrigation), with a maximum increase of 99 mS/m at 25 m along the transect, relative to baseline (Figures 13A-13D). At 6.0 m DOI, the EC_a responses at this location drops to 40 mS/m below baseline (Figure 13F). At Pecan_fine_5R (~61 m) on 5/9/2023 and 9/2/2023, there is a spike in EC_a responses spatially along the transect relative to baseline at 0.375, 0.75, and 1.5 m DOI (Figures 13A-13C), a dip at 3.0 m DOI (Figure 13D), and an increase at 6.0 m DOI (Figure 13E). At Pecan_coarse_5R (~88 m), EC_a responses on 5/9/2023 are lower by only ~8-17 mS/m relative to baseline across all DOI. Conversely, on 9/2/2023, EC_a responses at Pecan_coarse_5R are lower than baseline at 0.375 and 0.75 m DOI (by 1-14 mS/m), and higher at 1.5, 3.0, and 6.0 m DOI (by 4, 14, and 33 mS/m, respectively).

High frequency time series results reveal that EC_a responses generally decrease over time across all depths. However, EC_a responses recorded on 9/12/2023 were ~2 mS/m higher than those recorded 9/10/2023 at depths of 0.375 and 0.75 m (Figures 12A-12B). All graphs displaying high frequency sampling results show that EC_a responses approached maximum values near ~74 m (167.703 mS/m at 0.75 m DOI on 9/2/2023), and minimum values at ~90 m (13.061 mS/m at 0.375 m DOI on 9/8/2023) (Figures 12B and 12A, respectively). Additionally, peaks in EC_a responses

on 9/2/2023 and 9/28/2023 show large spatial changes between data collected along the transect at 15, 25, 45, 52, and 73 m that increase with depth at 0.375, 0.75, and 1.5 m DOI: ~100-150 mS/m at 0.375 m, 125-180 mS/m at 0.75 m, 152-220 mS/m at 1.5 m (Figures 12A-12C).

4.1.2 Magnetic Susceptibility Survey

Data from the magnetic survey show an area of high and low MS_a central to the site, indicating a magnetic anomaly (Figure 10F). Along the west and east edges of the site, there are high MS_a and low EC_a (Figures 10F and 10E, respectively). Low MS_a values are observed along the southeast, south, and southwest edges of the site.

4.2 IVEY PECAN ORCHARD

4.2.1 Electromagnetic Induction Surveys

Monthly EMI measurements along the 100 m transect show a general EC_a decrease over time. The first irrigation event on 6/13/2022 (data recorded on 6/24/2022) produced the highest EC_a responses across all depths, with values that peaked around 260 mS/m at 0.375 m DOI (Figure 14A). Furthermore, the highest monthly EC_a responses along the transect are consistently observed near Pecan_fine_Ivey (~41 m) and near 67 m from 0.375-3.0 m DOI (Figures 14A-14D). The lowest EC_a responses were collected on 10/28/2022 (41 days following the final irrigation event) with values around 8 mS/m at 0.375 m (Figure 14A). The lowest monthly EC_a responses along the transect are recorded near Pecan_coarse_Ivey (~18 m) and 82 m at DOI of 0.375-3.0 m (Figures 14A-14D).

High frequency measurements along the 100 m transect show a general EC_a decrease over time. Measurements near the Pecan_coarse_Ivey (~18 m) and Pecan_fine_Ivey (~41 m) locations show that the high frequency signal decreased by approximately the same amount (4 and 2 mS/m, respectively) during one irrigation event (Figures 15A-15E). There is a sharp decrease in the EC_a

response lateral to the Pecan_fine_Ivey location from 0.375-3.0 m DOI (Figures 15A-15D). Monthly and high frequency graphs at 3.0 and 6.0 m have sharp spatial changes, but consistent temporal EC_a responses (Figures 14D-14E and 15D-15E).

EC_a data collected on 6/24/2022 and 9/5/2022 were normalized to data collected on 10/28/2022 to show baseline shifts from the driest date of data collection (Figure 16). On 6/24/2022, EC_a responses at Pecan_fine_Ivey trend towards baseline as a function of depth: +127.64, +98.13, +82.15, +38.25 and -6.00 mS/m at 0.375, 0.75, 1.5, 3.0, and 6.0 m DOI, respectively. However, the EC_a responses at Pecan_fine_Ivey on 9/5/2022 relative to baseline do not follow the same pattern with depth; values of +48.06, +54.22, +73.09, +44.50, and +8.25 mS/m are observed at 0.375, 0.75, 1.5, 3.0, and 6.0 m DOI, respectively. Near 50 and 80 m, small baseline shifts of -0.75 mS/m to +17.76 mS/m are observed on 9/5/2022 at all except the 6.0 m DOI; where the EC_a responses dipped as low as -46.25 mS/m below baseline. Generally, data collected on 6/24/2022 show more variation and higher overall EC_a responses than data collected on 9/5/2022 relative to baseline at all except 6.0 m DOI (where differences are nominal). On 6/24/2022, the EC_a responses at Pecan_coarse_Ivey (~18 m) get closer to those documented on 10/28/2022 as depth increases: +55.77, +26.41, +10.71, +10.50, and +4.75 mS/m, at 0.375, 0.75, 1.5, 3.0, and 6.0 m DOI, respectively. An almost identical pattern is observed at Pecan_coarse_Ivey on 9/5/2022, but with overall lower EC_a responses relative to baseline: +26.38, +18.79, +5.71, +4.50, and +6.50 mS/m at 0.375, 0.75, 1.5, 3.0, and 6.0 m DOI, respectively.

4.2.1.1 1-Dimensional Inversion

The modeled EC data at Pecan_fine_Ivey on 9/6/2023 closely matches the soil sensor bulk EC data with a 0.14% RMS (Figure 18A). The modeled ECs agree within 0.97 mS/m or less (-3.90% or less difference; 0.487 mS/m standard deviation) across all layers relative to the corresponding

known soil sensor data (Figure 19A). At 0.3 m, the modeled EC is 57.21 mS/m (0.97% difference), increases to 105.597 mS/m from 0.45 to 0.75 m (0.60% difference), decreases to 20.408 mS/m from 0.75 to 1.05 m (0.16% difference), then increases slightly to 25.974 mS/m from 1.05 to 1.35 m (-3.90% difference). Soil sensor data were not available at 1.5 m depth; however, the modeled EC from 1.35 to 1.65 m is similar to the layer above at 24.691 mS/m. From 1.65 to 3.65 m, the EC increases dramatically to 531.915 mS/m and decreases in the half-space to 333.333 mS/m. The 1.2 m deep layer displays the greatest standard deviation across all layers (0.487 mS/m). The layer with the least standard deviation is directly above that, with a standard deviation of 0.016 mS/m. The VWC was 0.30 m^3/m^3 at 0.3 m, dropped to 0.29 m^3/m^3 at 0.6 m and to 0.23 m^3/m^3 at 1.2 m, and increased to 0.27 m^3/m^3 at 1.5 m.

The plot displaying the Pecan_fine_Ivey EC data on 7/16/2022 shows that the modeled EC is slightly higher than the soil sensor bulk EC data at corresponding depths (model RMS is 0.04%) (Figure 18B). The greatest variation between the modeled and sensor EC is at 0.9 m, where the percent difference is -15.54%. The soil sensor bulk EC shows an increasing trend from 0.3 to 0.9 m, ranging between 213.69 to 220.80 mS/m. In contrast, the modeled EC exhibits an initial increase from 0.3 to 0.6 m, followed by a decrease from 0.6 to 0.9 m, with values fluctuating between 242.718, 230.947, and 255.102 mS/m. The VWC increased with depth from 0.45 m^3/m^3 at 0.3 m to 0.52 m^3/m^3 at 0.6 m. Subsequently, the VWC decreased to 0.47 m^3/m^3 at 0.9 m, 0.40 m^3/m^3 at 1.2 m, and most notably, values decreased to 0.04 m^3/m^3 at 1.5 m.

From 7/16/2022 to 9/6/2023 at Pecan_fine_Ivey, EC and VWC decrease in every layer; both in the modeled and soil sensor data (Figures 18A and 18B). The greatest variability in the modeled EC is in the half-space layer, where the EC increases from 75.245 to 333.333 mS/m,

followed by the 4th layer (~0.75 m), where the EC decreases from 255.212 to 20.408 mS/m. The modeled EC changes the least over time ~1.2 m, where values vary only 3.65 mS/m.

The modeled EC data from Pecan_coarse_Ivey on 9/6/2023 ranges in accuracy relative to the available sensor data corresponding depths (0.05% RMS) (Figure 18C). The modeled EC in the top 0.36 m thick layer is 9.99 mS/m, then decreases to 8.15 mS/m from 0.36 to 0.96 m. No sensor data are available at the 0.3 and 0.6 m depths for comparison. From 0.96 to 1.46 m, the modeled EC increases drastically to 93.98 mS/m, a -8.85% difference from the nearby 0.9 m deep sensor with an EC of 86.34 mS/m (Figures 18C and 19C). The greatest difference between modeled and sensor EC is at 1.2 m (95.90% difference) with a 39.336 mS/m standard deviation (Figure 19C). From 1.46 to 2.43 m, the modeled EC was 100 mS/m, a 33.11% difference from the 149.5 mS/m recording at the 1.5 m soil sensor. VWC data available at 0.9, 1.2, and 1.5 m were 0.20, 0.26, and 0.42 m^3/m^3, respectively.

On 7/16/2022, the Pecan_coarse_Ivey modeled EC (RMS of 0.03%) was the highest from 0.36 to 0.96 m, after which it decreased to less than 5 mS/m in the remainder of the column (Figure 18D). However, collected bulk soil sensor EC data do not reflect the same pattern: The 0.3 and 0.6 m sensor data were 9.85 and 2.00 mS/m, respectively, after which it increased relatively linearly to 154.20 mS/m at 1.5 m. The greatest difference in modeled versus soil sensor EC is at 0.6 m (-5,145.59%). While the modeled data between 0.96 and 2.43 m range between 95.15%-96.76% different from soil sensor bulk EC data, both show a linear trend as the depth increases, with the soil sensor bulk EC increasing more at depth relative to the modeled EC data. The VWC was 0.21 m^3/m^3 at 0.3 m, 0.31 m^3/m^3 at 0.6 m, 0.20 m^3/m^3 at 0.9 m, 0.26 m^3/m^3 at 1.2 m, and 0.42 m^3/m^3 at 1.5 m depth.

At Pecan_coarse_Ivey, the modeled EC from 7/16/2022 to 9/6/2023 exhibits a trend reversal between the second and third layers (0.36-0.6 m, and 0.6-0.96 m) (Figures 18C and 18D). The modeled EC decreases in the second layer from 104.93 to 8.15 mS/m, and increases in the third layer from 2.90 to 93.98 mS/m. Over time, the layer with the least modeled EC change is from 1.46 to 2.43 m, where the EC decreased from 3.37 to 3.10 mS/m. The greatest changes in modeled EC over time are from 2.43 m to the half-space, where the EC increased from 5 to 100 mS/m, followed closely by the third and second layer, respectively. The VWC data available at 0.9, 1.2, and 1.5 m depths did not change at all between the two dates.

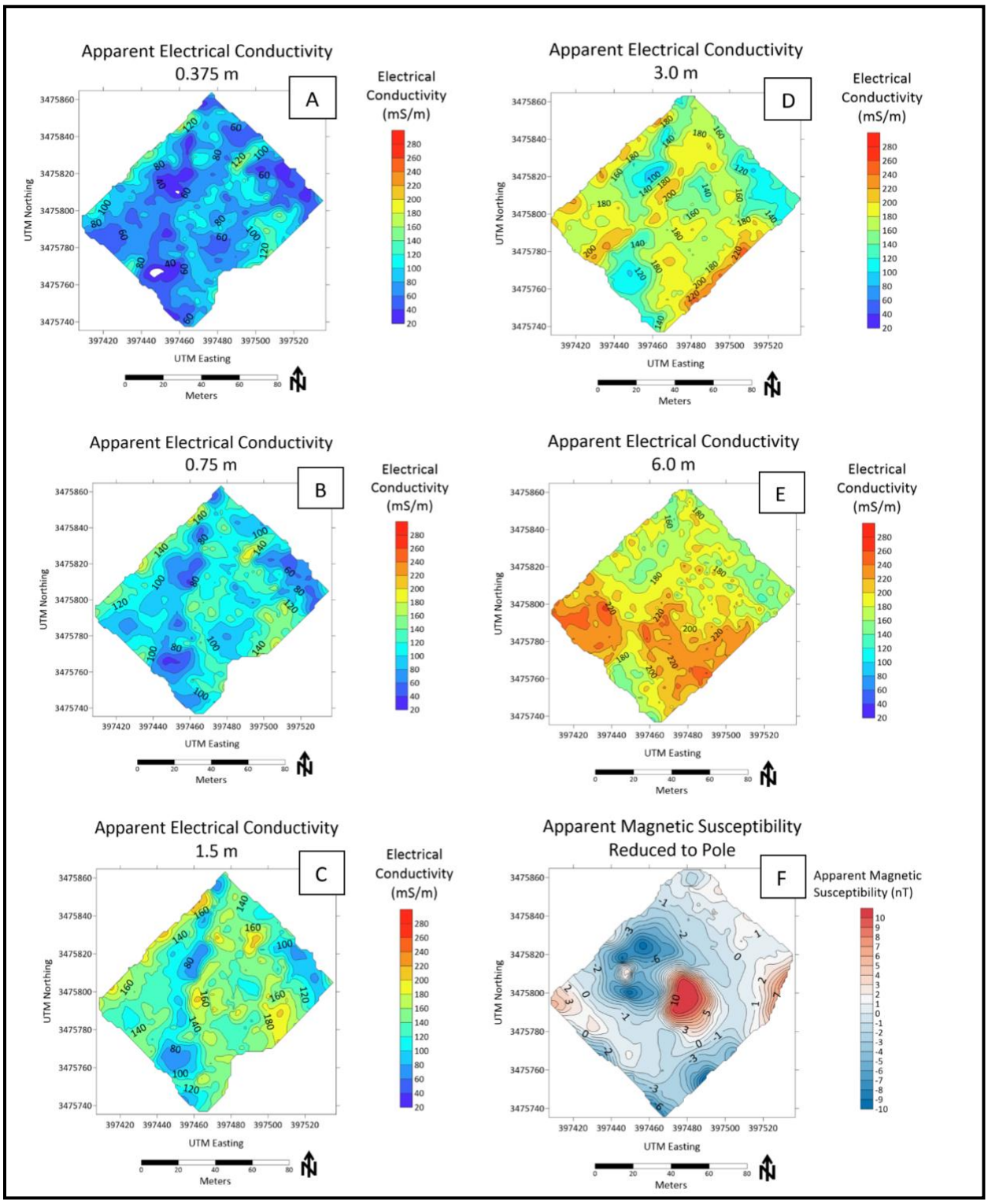

Figure 10: Pre-irrigation surveys of 5R (A-E) on March 16-17, 2022, displaying recorded EC_a at different depths and (F) on April 13, 2022 displaying recorded MS_a that were reduced to the pole and relative to the earth's ambient magnetic field (46,647.9 nT) at the time of the survey.

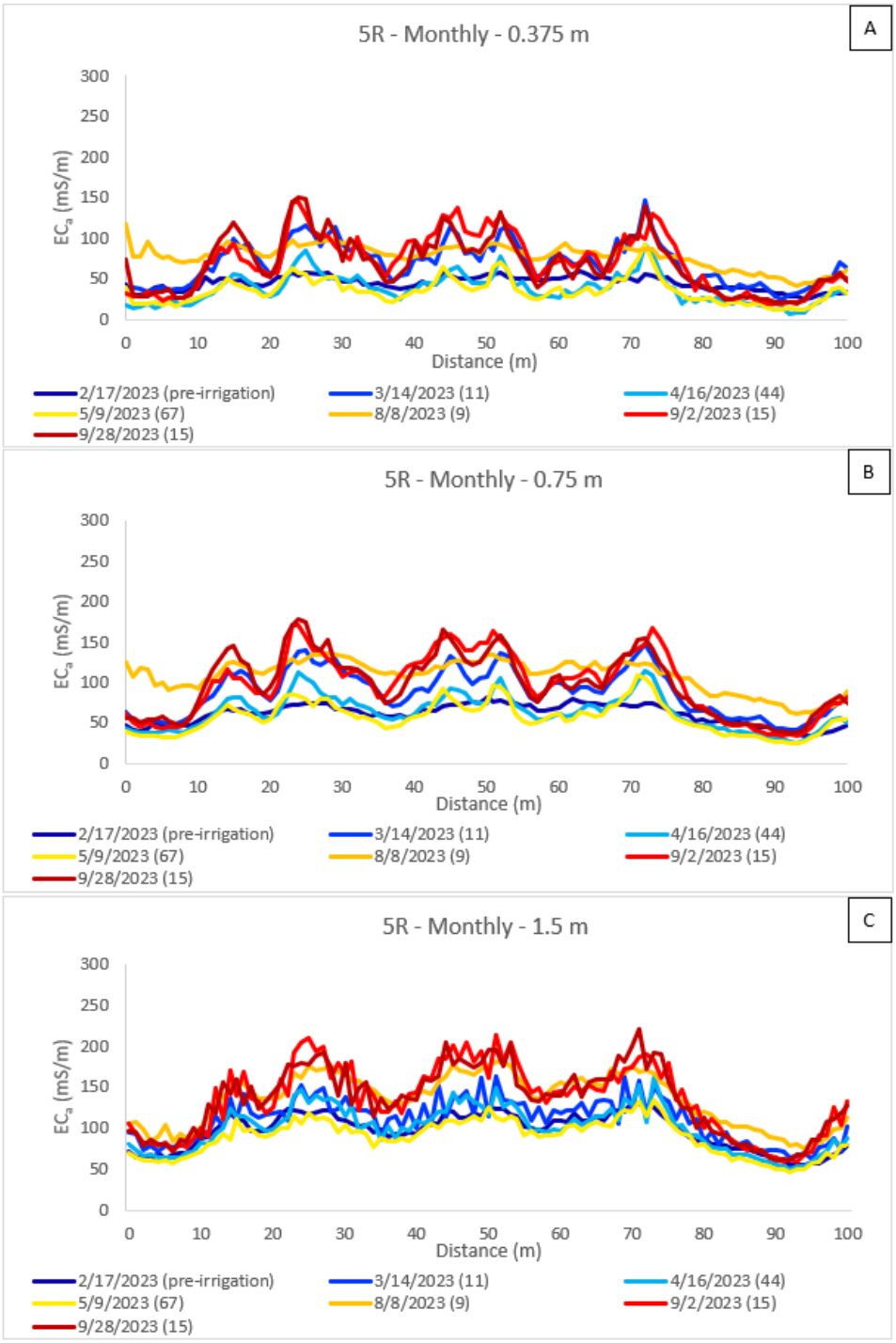

Figure 11: (A-C) Monthly time series data collected across a 100 m transect (green line in bottom image) before and during irrigation season at 5R. Red dot indicates Pecan_fine_5R soil sensor location (~61 m) and yellow dot indicates Pecan_coarse_5R soil sensor location (~88 m). The legend displays the date of data collection and number of days since the most recent irrigation in parenthesis.

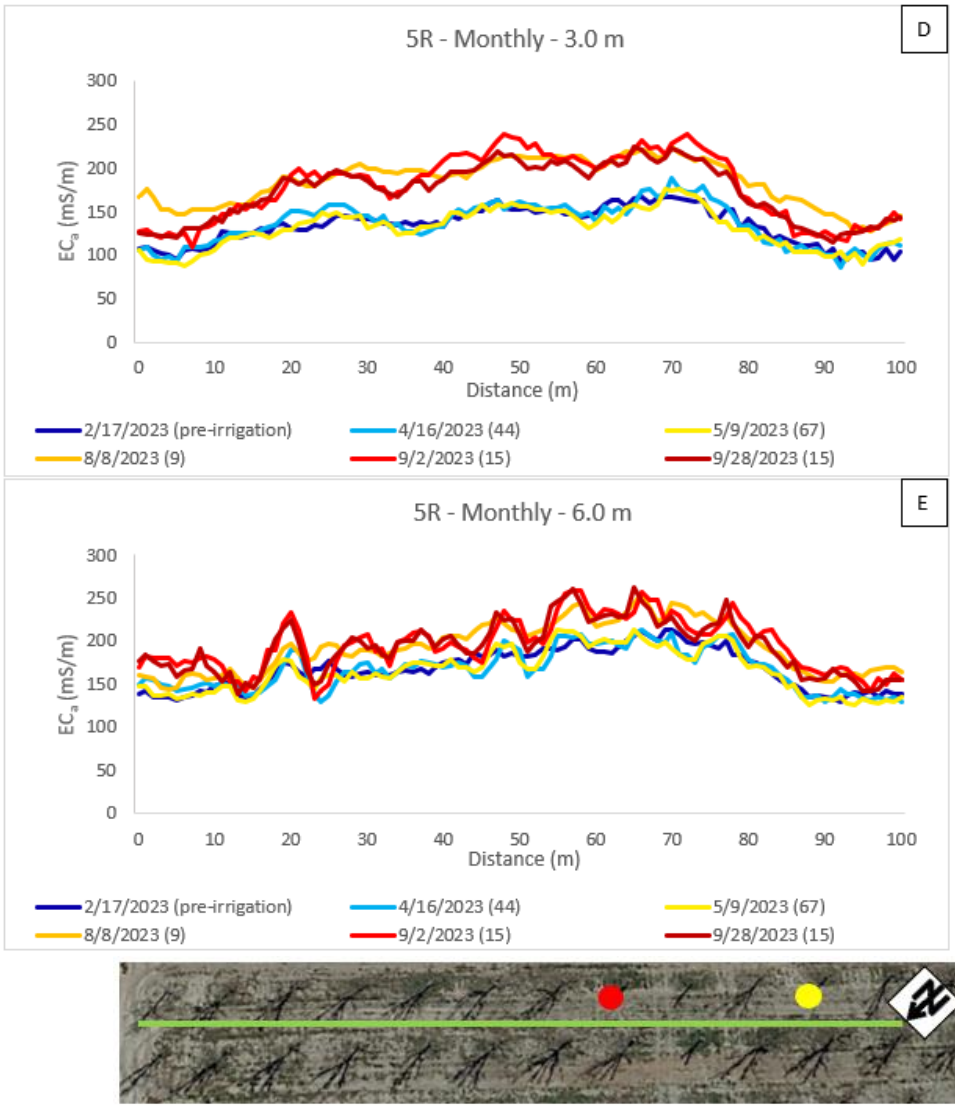

Figure 11: (D-E) Monthly time series data collected across a 100 m transect (green line in bottom image) before and during irrigation season at 5R. Red dot indicates Pecan_fine_5R soil sensor location (~61 m) and yellow dot indicates Pecan_coarse_5R soil sensor location (~88 m). The legend displays the date of data collection and number of days since the most recent irrigation in parenthesis.

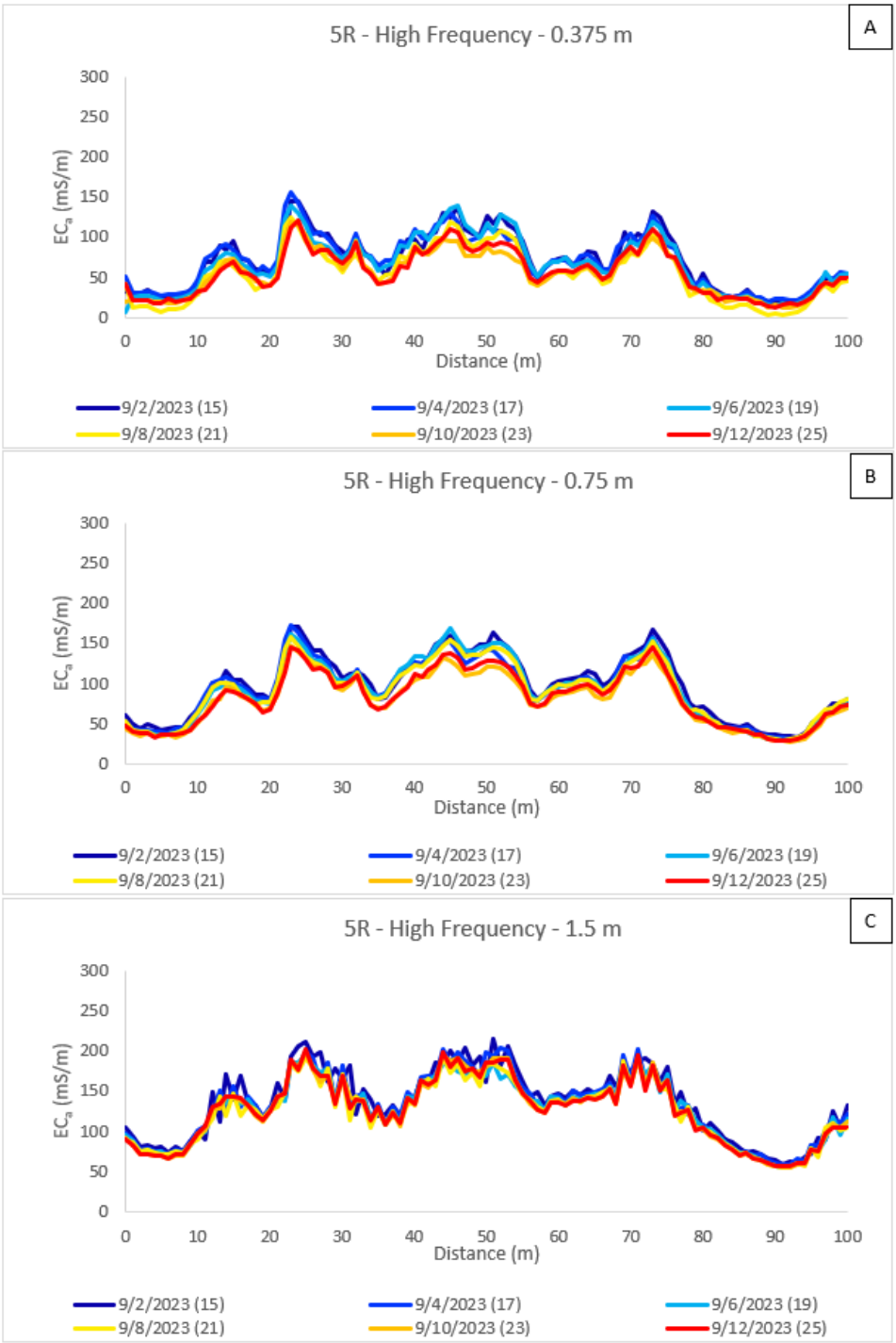

Figure 12: (A-C) High frequency time series data collected at 5R every other day in September 2023. Data collection began 15 days after an irrigation and stopped the day before the following irrigation. Data were collected across the same 100 m transect as the monthly survey.

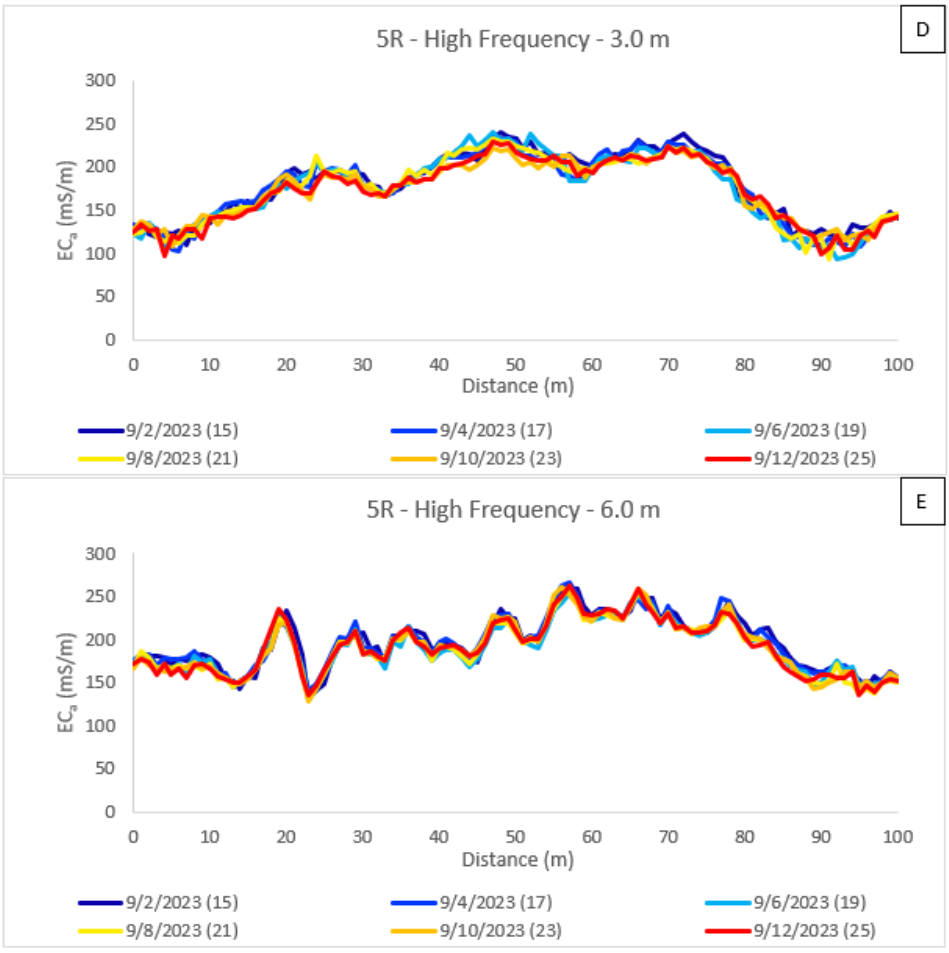

Figure 12: (D-E) High frequency time series data collected at 5R every other day in September 2023. Data collection began 15 days after an irrigation and stopped the day before the following irrigation. Data were collected across the same 100 m transect as the monthly survey.

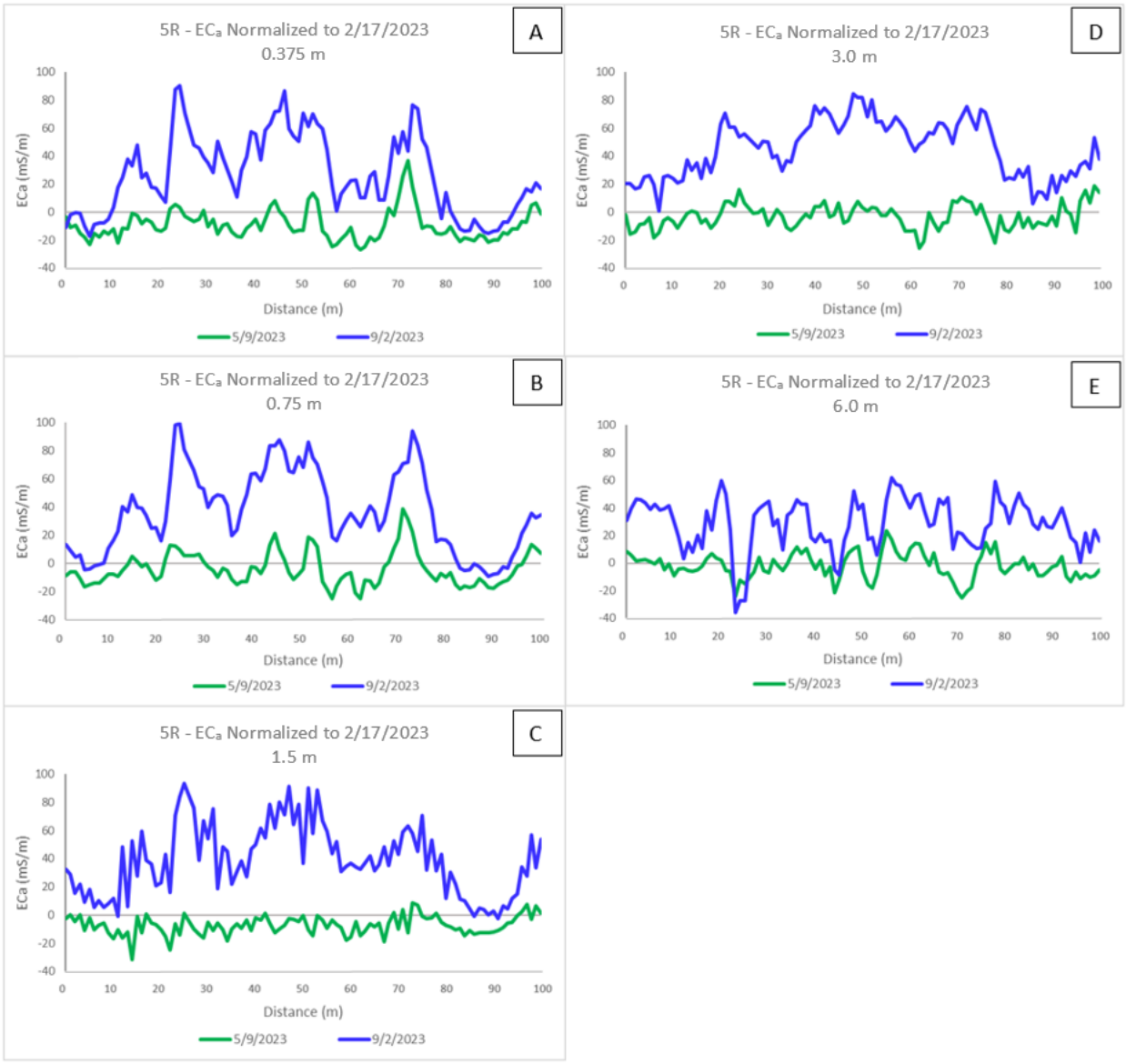

Figure 13: Time series data from 5R normalized to 2/17/2023 prior to the irrigation season beginning. Data collected on 5/9/2023 were recorded 67 days after an irrigation, and data collected on 9/2/2023 were recorded 15 days after irrigation.

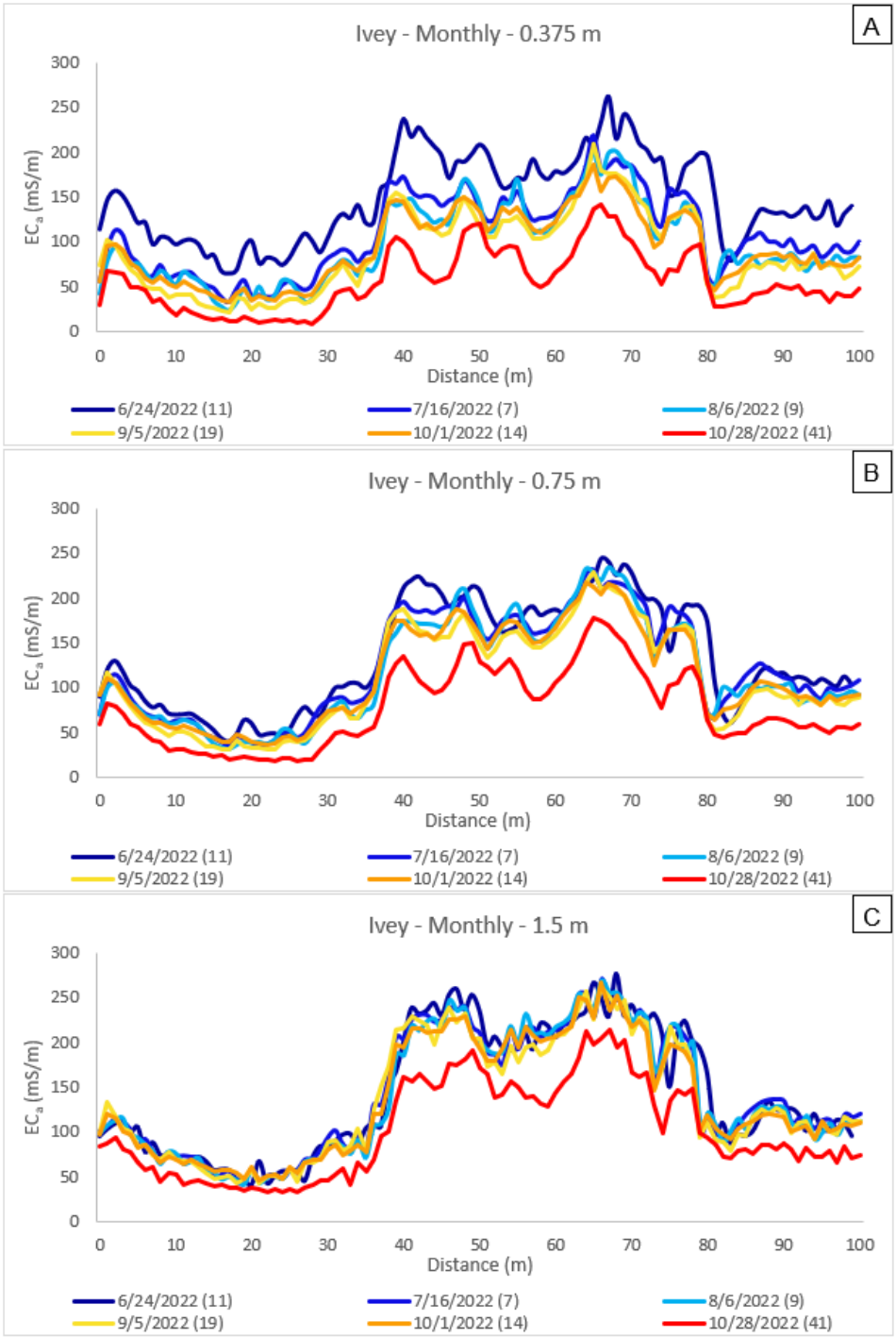

Figure 14: (A-C) Monthly time series data collected across a 100 m transect (blue line in bottom image) before and during irrigation season at Ivey. The yellow dot indicates Pecan_coarse_Ivey soil sensor location (~18 m) and the red dot indicates Pecan_fine_Ivey soil location (~41 m). The legend displays the date of data collection and number of days since the most recent irrigation in parenthesis.

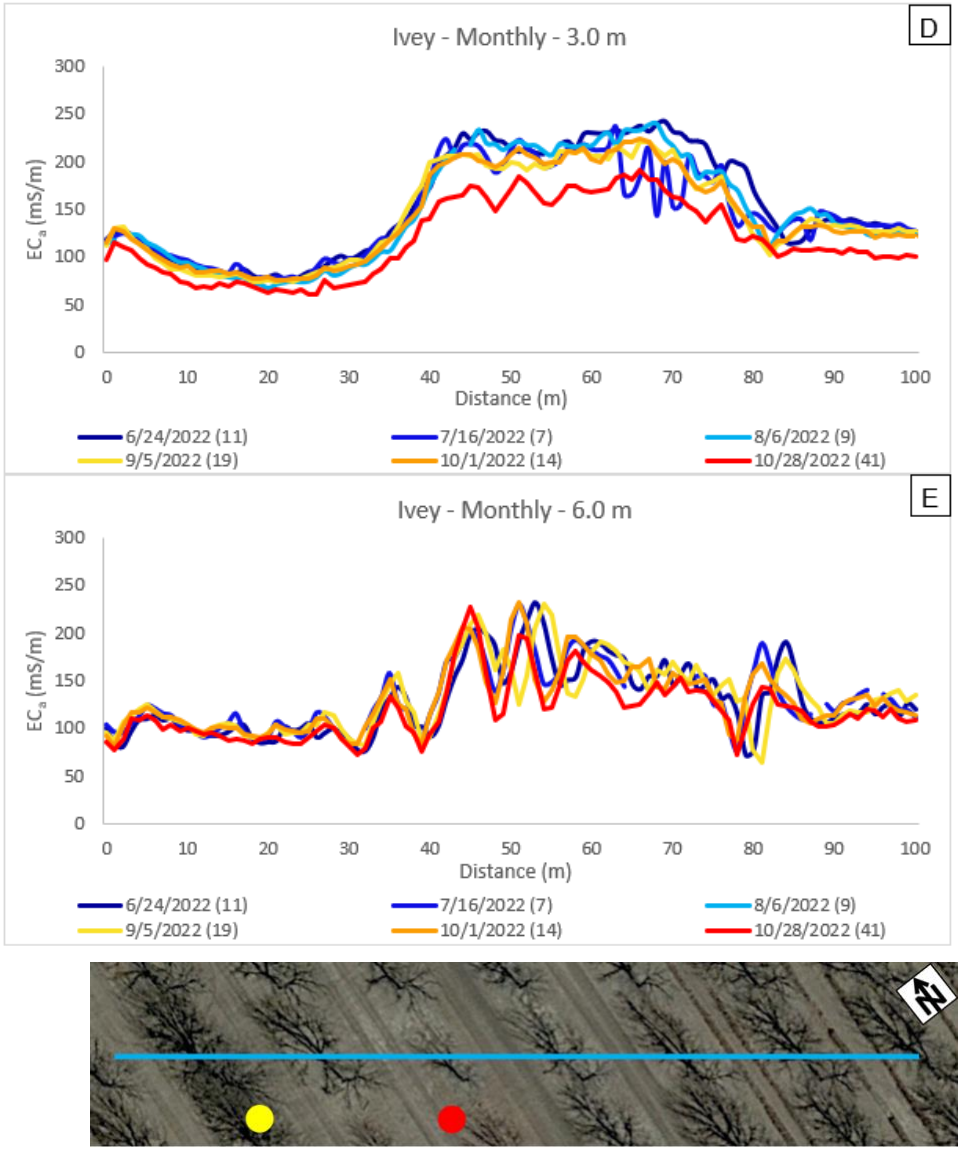

Figure 14: (D-E) Monthly time series data collected across a 100 m transect (blue line in bottom image) before and during irrigation season at Ivey. The yellow dot indicates Pecan_coarse_Ivey soil sensor location (~18 m) and the red dot indicates Pecan_fine_Ivey soil location (~41 m). The legend displays the date of data collection and number of days since the most recent irrigation in parenthesis.

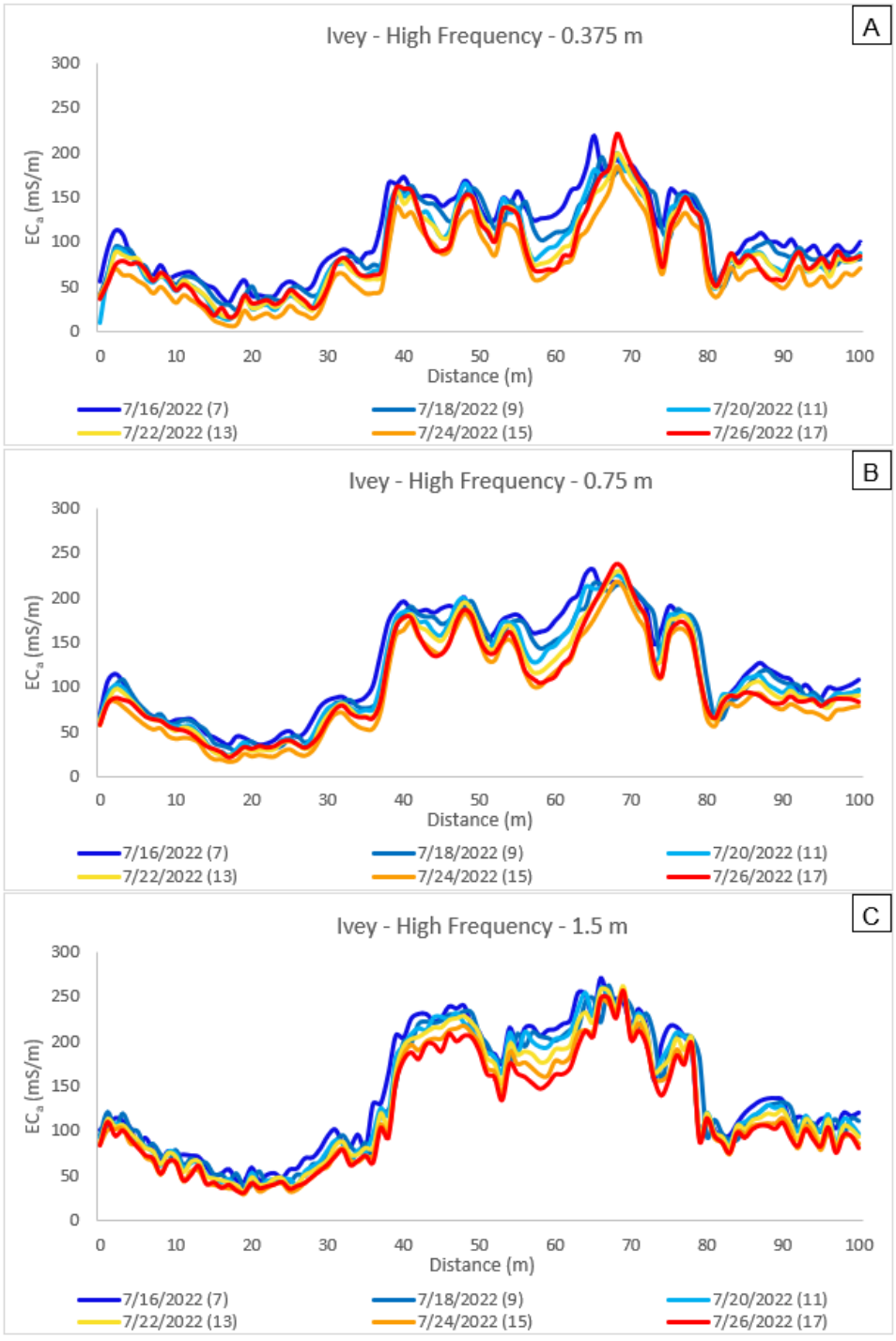

Figure 15: (A-C) High frequency time series data collected at Ivey every other day in July 2022. Data collection began ~6 days after an irrigation and stopped the day before the following irrigation. Data were collected across the same 100 m transect as the monthly survey.

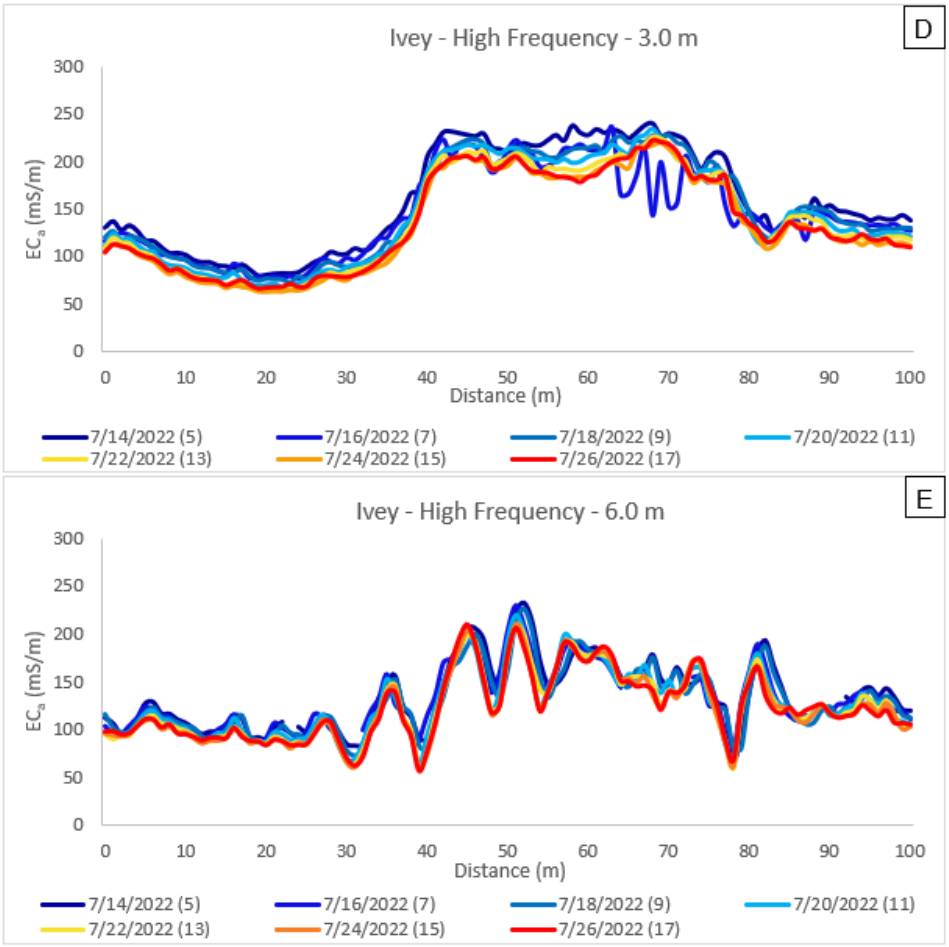

Figure 15: (D-E) High frequency time series data collected at Ivey every other day in July 2022. Data collection began ~6 days after an irrigation and stopped the day before the following irrigation. Data were collected across the same 100 m transect as the monthly survey.

Figure 16: Time series data from Ivey normalized to 10/28/2022, when the soil was the driest of all recorded days. Data collected on 6/24/2022 were recorded 11 days after irrigation and data collected on 9/5/2022 were recorded 19 days after irrigation.

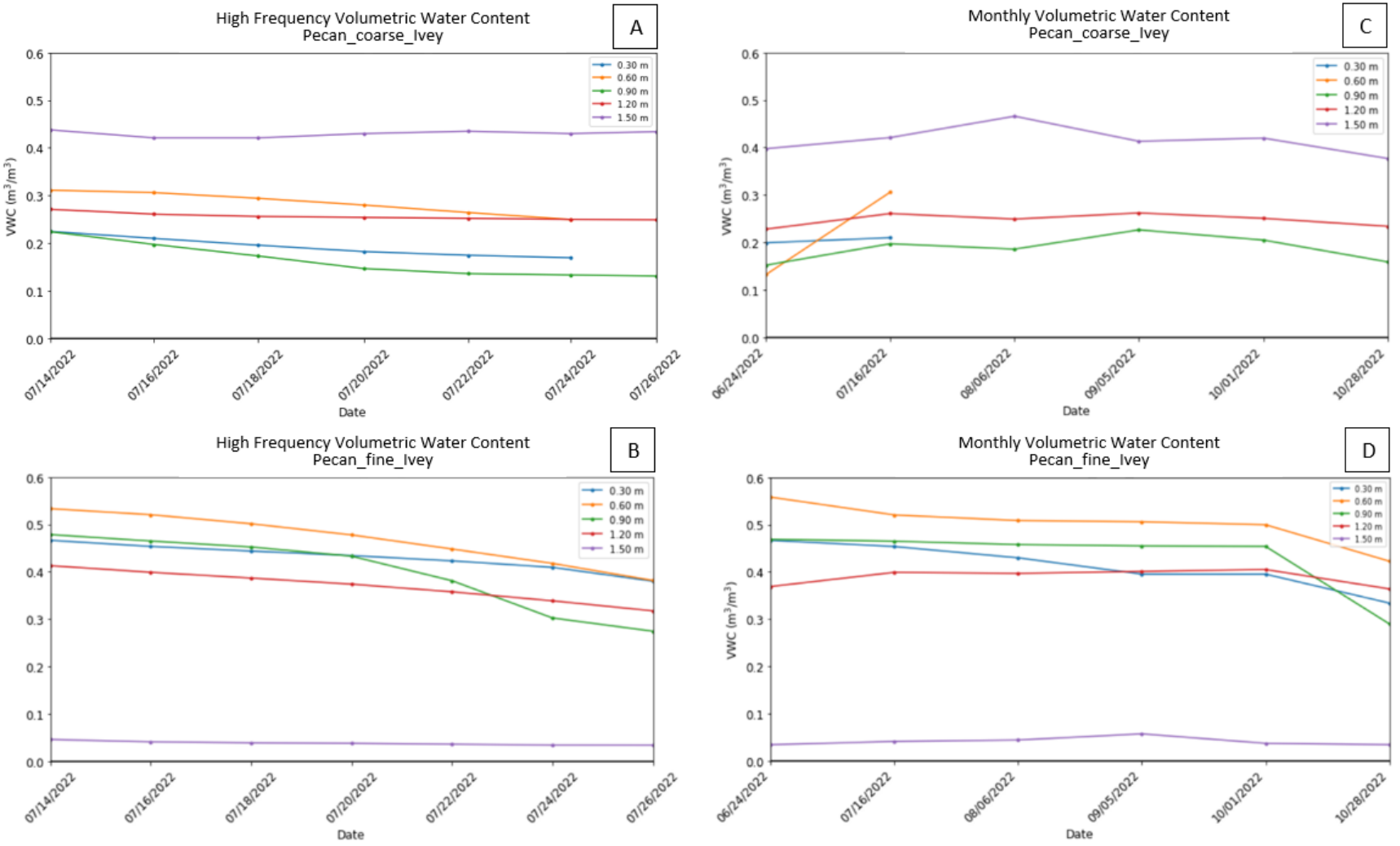

Figure 17: Soil sensor volumetric water content data collected at Ivey's Pecan_coarse_Ivey and Pecan_fine_Ivey sites (A-B) every other day in July 2022 and (C-D) monthly from June 2022-October 2022. Date and time of collection coincide with EMI data collection. Depths of data collection are at 0.3, 0.6, 0.9, 1.2, and 1.5 m. No soil sensor data is available at the 0.30 and 0.60 m depths from 7/26/2022-10/28/2022.

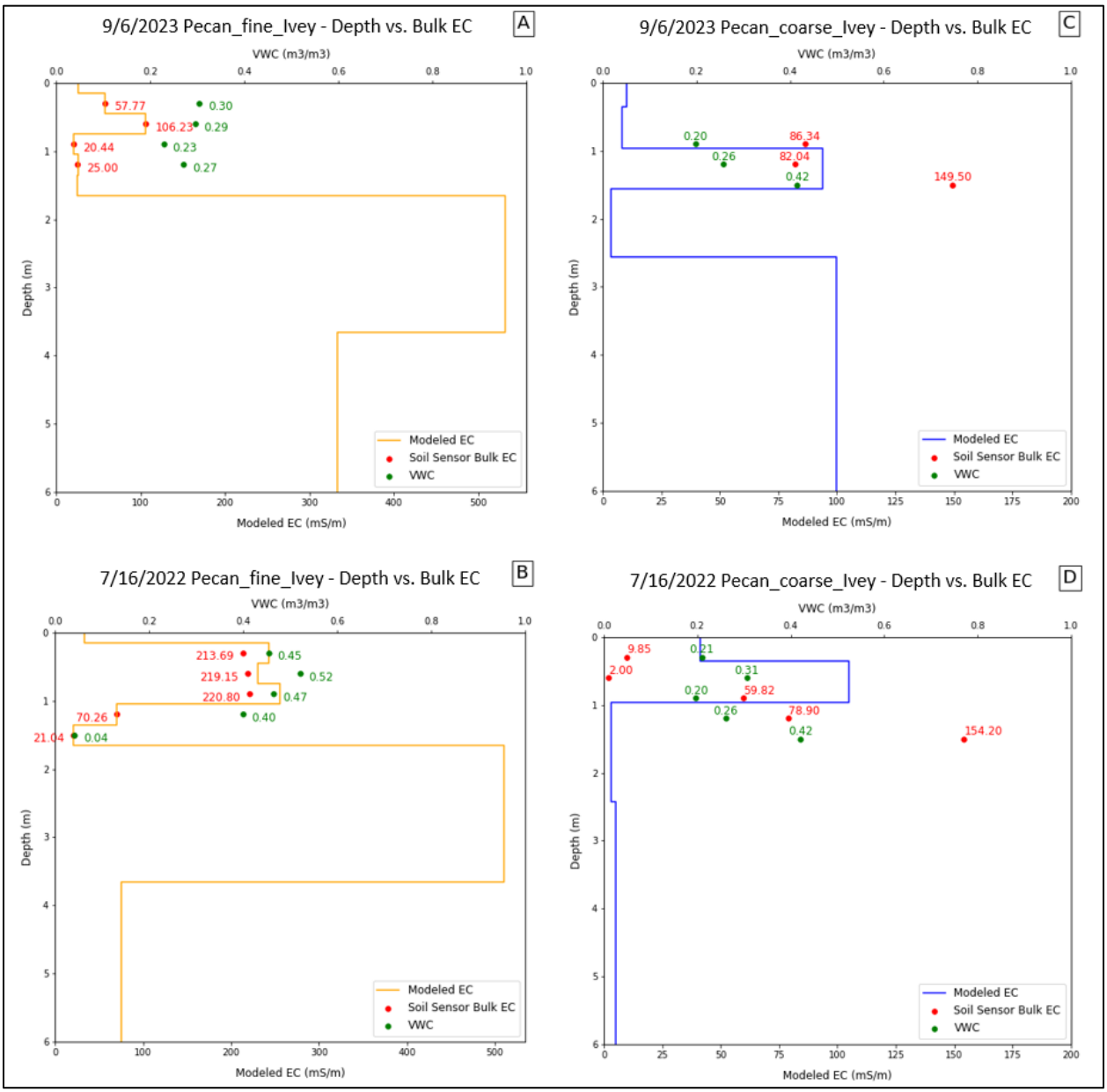

Figure 18: Plots of the modeled depth vs soil sensor bulk EC at Ivey site on (A) 9/6/2023 at Pecan_fine_Ivey, (B) 7/16/2022 at Pecan_fine_Ivey, (C) 9/6/2023 at Pecan_coarse_Ivey, and (D) 7/16/2022 at Pecan_coarse_Ivey. The soil sensors are at depths of 0.3, 0.6, 0.9, 1.2, and 1.5 m. Volumetric water content (green dots) are displayed at corresponding depths where soil sensor bulk EC are recorded.

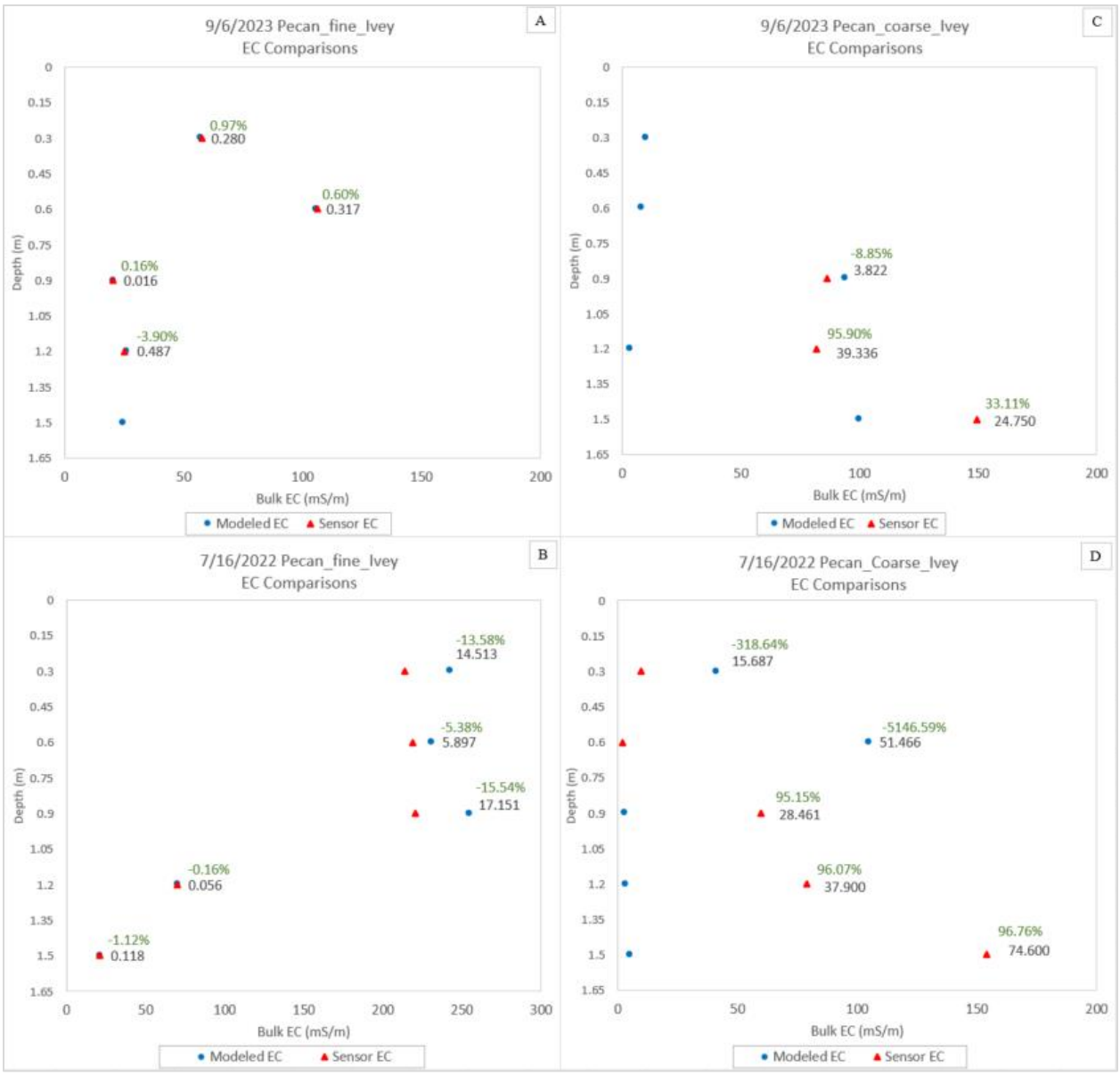

Figure 19: Comparisons between modeled EC and soil sensor bulk EC at Ivey site on (A) 9/6/2023 at Pecan_fine_Ivey, (B) 7/16/2022 at Pecan_fine_Ivey, (C) 9/6/2023 at Pecan_coarse_Ivey, and (D) 7/16/2022 at Pecan_coarse_Ivey. The green percentage is the percent difference between the modeled EC and the soil sensor bulk EC measured at the corresponding layer. The black number is the standard deviation between the modeled EC and the soil sensor bulk EC at the corresponding layer.

Section 5: Discussion

5.1 Controls on EC_a as determined from time series results

Observations from time series sampling using EMI instruments indicate that there are both static (i.e., spatial) and temporal variations in EC_a signals at both sites. Where static factors (e.g., soil texture) controlling the magnitude of EC_a are dominant, spatial patterns tend to remain constant over time (Johnson et al., 2003, Corwin & Lesch, 2005). Large-grained soils, which have lower surface electrical charge, lower surface-to-volume ratios, high porosity, high permeability, and low water holding capacity, respond to changes in water content relatively quickly, resulting in relatively low EC_a responses under most conditions (Heil & Schmidhalter, 2011).

Relatively time-constant EC_a responses throughout the irrigation season are a major feature of EMI data across the transects at 5R and Ivey, pointing to correlations between EC_a response and soil texture. For example, consistently low EC_a values across all DOI at the time of the March 2022 baseline survey observed at 5R's Pecan_coarse_5R site (~88 m) suggests electromagnetic signals correspond to a coarse soil. Time series data at this same site exhibit static patterns where the EC_a responses vary minimally from the pre-irrigation season to its conclusion (Figures 10A-10E and 13A-13E) supporting the interpretation that the EC_a signal is dominated by soil texture rather than moisture or salinity. This interpretation is reinforced by soil texture data from Pecan_coarse_5R, revealing that the initial 0.75 m of the subsurface consists of 45-57% sand (Jessica Hartman & Frida Garcia Ledezma, personal communications, 2023).

At Ivey, the monthly time series EC_a data recorded near Pecan_coarse_Ivey (~18 m) are the lowest observed along the transect (~12-76 mS/m from 0.375-3.0 m DOI). Such observations suggest that coarse-textured soils drain quickly, producing low EC_a responses (Figures 14A-14D). This interpretation is supported by soil EC data from a soil water slurry indicating that the soil at

0.40 m is 0.466 dS/m (Ortiz & Jin, 2021). Additionally, Sosa's 2019 2D resistivity survey and Garcia's 2021 EMI survey across the 100 m transect show that corresponding areas of sandier soils have EC_a values ranging from 60-130 mS/m after the irrigation events near the start of the growing season, fostering the interpretation that over three years of irrigation events, areas that consistently yield lower EC_a responses are driven by coarse soil textures (Sosa 2019; Garcia, 2021). Garcia (2021) correlated these areas to good/positive tree growth suggesting that coarse soil texture supported the drainage of irrigation water and increased flushing of salts away from the tree roots. Furthermore, the minimal EC_a variations over time observed at Pecan_coarse_Ivey and at points of 37 m and 83 m along the transect align with Pecan_coarse_Ivey soil texture samples that show sand is the dominant texture (ranging from 44-97% sand) throughout the 3.0 m borehole, and therefore is the main control on the EC_a response (Figure 16).

Recurrent high EC_a responses in time series data and data normalized to baseline at both sites can be attributed to fine textured soils dominating EC_a responses. Finer-textured soils are characterized by greater surface electrical charge, higher surface-to-volume ratios, small particle size, high clay content, high surface area, reduced pore space, and therefore slow drainage, soliciting high EC_a responses (Heil & Schmidhalter, 2011; Jaja, 2016; Doser et al., 2019). This interpretation is apparent in September 2023 at 5R, for data collected at locations of 25, 47, and 73 m along the transect from 0.375-3.0 m DOI (Figures 12A-12D). These locations showcase a correlation between finer textures and consistently elevated EC_a responses, underscoring the relationship between the two characteristics. These same three locations along the transect show the highest EC_a responses along the entire transect when data from 9/2/2023 are normalized to data from 2/17/2023. I hypothesize that these increases are a direct result of greater water-holding and slow drainage characteristics of finer soils post irrigation (Figures 13A-13D). Consistent peaks

and troughs in EC_a responses over time at the 6.0 m DOI indicate stable water content, emphasizing the predominant influence of soil texture on EC_a responses, where peaks suggest finer textures, while valleys suggest coarser textures (Figure 12E). The observed see-saw pattern with minimal variations over several months at measurement points from 38 to 80 m along the transect and for all DOI suggest that in areas where consistently high EC_a responses are focused, finer-textured soils are located, controlling the EC_a response (Figures 11A-11E).

Similar patterns are also observed at Ivey, where relatively high EC_a responses fluctuate minimally over time at Pecan_fine_Ivey (~41 m) and measurements near 67 m along the transect (Figures 15A-15E). This interpretation is supported by previously recorded EC_a data at the Pecan_fine_Ivey borehole at 1.5 m DOI where higher conductivity values corresponded to the increase in clay content to 70% at 1.0 m depth (Garcia, 2021). The non-uniform movement of water, and thus textural controls on EC_a, is evidenced by the sharp decrease in EC_a responses near Pecan_fine_Ivey from 0.375-3.0 m DOI (Figures 15A-15D). These observations indicate that water seeks preferential flow paths that drain laterally from the finer-grained clay into nearby coarser-grained pockets, agreeing with the general nature of water flow in unsaturated conditions (Hendrickx & Flury, 2001). Additionally, high frequency data from 5R reveal possible focused, preferential flow paths near measurement points at 25, 47, and 73 m along the transect where the EC_a response drops along the transect following irrigation (Figures 12A-12C).

In areas where dynamic soil properties (e.g., variable salinity and water content) exert a greater influence on EC_a responses, temporal shifts in spatial patterns exhibit more fluidity (Johnson et al., 2003a; Corwin & Lesch, 2005). Based on results from high frequency time series surveys (Figures 12 and 15), the primary factor controlling temporal EC_a variations is water content, where uniform decreases in EC_a over time are likely a result of soils drying out following

the most recent irrigation (Figure 17). This interpretation is consistent with observations at Ivey's Pecan_coarse_Ivey and Pecan_fine_Ivey locations, where the EC_a decreased by 4 and 2 mS/m, respectively, between each subsequent date of data collection (Figures 15A-15E). Following this logic, the anomalously high EC_a responses seen at 0.375 and 0.75 m DOI on 7/26/2022 can be attributed to the 3.30 and 8.89 mm of rain the field received on 7/25/2022 and 7/26/2022, respectively (Figures 15A and 15B), which led to an increase in EC_a only in the upper few decimeters in the soil due to the limited infiltration.

At 5R, incremental decreases in high frequency EC_a responses are observed at the 0.375, 0.75, and 1.5 m DOI (Figures 12A-12C). However, at 3.0 m DOI, the EC_a responses are less distinguishable across dates, and even increase throughout time at peaks observed near measurements near 24, 27, and 70 m along the transect, despite decreasing water content data across the field (Figure 12D). These high EC_a measurements that increase with time in response to one irrigation event indicate that soils at these locations do not drain well, and potentially accumulate water and/or salt even though no additional sources were introduced into the system. High frequency observations from both sites at 6.0 m DOI indicate that the EMI measurements capture EC_a responses below the groundwater table (~3.0 m) (Figures 12E and 15E). That is, EC_a responses at this depth do not decrease over time; instead they consistently yield the highest EC_a responses compared to any other depth, reflecting fully saturated soils from relatively brackish groundwater.

At 5R on 11/3/2023, the specific conductance was 10,100 μS/cm and TDS was 7,700 mg/L in very shallow (~3-5 m deep) groundwater (Mark Engle, personal communications, 2023). Relatively low and consistent EC_a responses at 5R observed on 2/17/2023 across all DOI can be attributed to dry, relatively vertically homogenous soil moisture conditions before the irrigation

season began, and a lack of precipitation the site received (Figure 11). Compared to this baseline, the EC_a responses observed at all DOI on 5/9/2023 exhibit minimal variations (Figure 13). On this date, 67 days had elapsed since the last irrigation, emphasizing the influence of soil moisture scarcity on corresponding temporal EC_a responses.

Changes in irrigation water sources throughout the growing season, with corresponding variations in salinity, lead to moderate variation in the EC_a responses. The majority of irrigation water sources of at Ivey in 2022 and 5R in 2023 were reported to be from the Rio Grande (TDS of 500-1,500 mg/L) (Table 1). At 5R, the first irrigation event on 2/17/2023 was likely sourced from deep groundwater (~30-50 m deep and TDS of 2,000-3,000 mg/L) (Santosh Palmate, personal communications, 2023). The irrigation water sources at Ivey on 4/23/2022 and 5/20/2022 are unknown, and from groundwater on 9/17/2022 (Ivey family, personal communications, 2023). Concomitant increases in EC_a immediately following irritation, regardless of the source water salinity, further points to the interpretation that soil water content, not salinity, has the largest control on EC_a responses over the course of this study. The 1.5 m of irrigation water each site receives annually (equivalent to 12.7 centimeters per event) significantly outweighs the relatively trivial mean annual precipitation of ~16-25 cm the region receives (Ortiz et al., 2022). This renders natural precipitation negligible in comparison to irrigation water as a water source and control on EC_a (with the exception of the afore mentioned anomalously higher EC_a observed at 0.375 and 0.75 m DOI at Ivey on 7/26/2022 when recent precipitation events added to the increase in EC_a responses).

The connection between soil texture, water content, and salinity on subsurface electromagnetic properties is highlighted through time across both sites, where a combination of variations in these static and time-dependent properties control EC_a responses. On 9/2/2023 at 5R,

following the seventh field irrigation of the season, areas with anomalously high EC_a relative to baseline conditions are interpreted to be intervals containing finer materials. These elevated EC_a responses may be a result of localized water accumulation due to slow drainage and/or precipitation of calcite and evaporite minerals from soil water evaporation (Figures 13A-13C). Precipitation of secondary minerals in these areas has the potential to further exacerbate salinity and water build-up due to soil pore clogging and further reduction of infiltration. A similar interpretation can be applied to the see-saw pattern at points 15, 25, 45, 52, and 73 m along the transect from 0.375 to 3.0 m DOI, where high EC_a responses may be the result of water retention due to inadequate drainage or areas of salt accumulation adjacent to sandier areas that drainage water more readily (Figures 11A-11D and 12A-12D).

At Ivey, the EC_a responses along the transect shift from relatively low (0.0-35 m) to high (35-78 m), back to low (78-100 m) (Figure 15). This interpretation is consistent with the observation that tree canopy size along the transect changes from smaller to larger to smaller, respectively, as a result of soil moisture levels and textural differences (Garcia, 2021). Additionally, EC_a data collected along the transect at the 1.5 m DOI exhibit the highest EC_a responses across all depths, which is consistent with results from Garcia (2021), who found that at the ~1.5 m DOI, generally high EC_a values likely correspond to small grain size and salt accumulation as a result of repeated flood irrigation (Figure 15C). This is also consistent with Ortiz & Jin (2021), who collected soil samples from Pecan_fine_Ivey that indicate from the 0.688-1.374 m depth, the pH ranges from 7.51-7.77 while the EC from a soil water slurry ranges from 2.776-3.68 dS/m.

The general increase of EC_a responses as depth increases can be attributed to soil water content increasing and soil texture varying as a function of depth. This is seen through high

frequency data at 5R where EC_a responses along the transect range from 13-155 mS/m at 0.375 m DOI, 36-172 mS/m at 0.75 m DOI, 56-201 mS/m at 1.5 m DOI, 97-241 mS/m at 3.0 m DOI, and 137-262 mS/m at 6.0 m DOI (Figures 12A-12E). 5R March 2022 baseline survey results show that at the 0.375, 0.5, and 1.5 m DOI there are generally low EC_a responses, which increase with depth (Figures 10A-10C). This trend indicates that a combination of factors, including evapotranspiration, minimal precipitation, and the absence of irrigation at that point in the season, collectively lead to low soil moisture content and relatively low EC_a responses. Soil texture data gathered from the Pecan_coarse_5R and Pecan_fine_5R sites reveal a predominantly silty composition and high soil pH between 2.5 to 3.0 m (50-82% silt and 7.72-8.27 pH at Pecan_coarse_5R; 59-71% silt and 7.73-8.18 pH at Pecan_fine_5R) (Jessica Hartman & Frida Garcia Ledezma, personal communications, 2023). This suggests that the abundant fine-grained silt particles possess the ability to have a high capillary rise and draw relatively saline groundwater upward from the groundwater table (~3.0 m deep), resulting in elevated EC_a values at the 3.0 m depth (~100-220 mS/m) (Figure 10D). At 6.0 m, the EC_a is very high (~140-260 mS/m), and remains consistently high throughout the season, likely due to the measurement's location below the groundwater table (~3.0 m) containing dissolved ions, and the integrated measurement from accumulated salts beneath the maximum average 1.83 m deep root zone (Abudu et al., 2016; Ortiz et al., 2022) (Figure 10E). At Ivey, a similar pattern of increasing EC_a responses with depth is seen in high frequency data, but with higher maximums than 5R at shallow depths: EC_a ranges from ~6-219 mS/m at 0.375 m DOI, ~21-237 mS/m at 0.75 m DOI, and ~30-270 mS/m at 1.5 m DOI (Figures 15A-15C).

Considering both sites received the same amount and source of irrigation water, it can be inferred that generally higher EC_a responses at Ivey than at 5R is a result of generally finer texture

in the soils at Ivey across all depths, and greater accumulation water and salts from 0.375 to 1.5 m DOI. At the 3.0 and 6.0 m DOI, the ranges in high frequency EC_a at Ivey are lower than the ranges observed at 5R (68-234 and 57-227 mS/m, respectively) (Figures 15D-15E). This suggests that the finer textures and the consequent accumulation of water and salt at shallower depths limit infiltration to deeper layers, resulting in lower EC_a responses at 3.0 and 6.0 m DOI.

5.2 Insights into layer specific EC_A from inversion modeling

The use of the inversion program to model EC at various points in time provides insight into site and layer-specific electrical conductivity responses to change in water content, texture, and salinity. A priori soil texture data, measured EC_a, and soil moisture EC were used to inform model parameters (i.e., layer resistivity, layer thickness and number of layers), which dictated the outcome of the modeled EC. Small changes in individual input parameter led to varied model EC outputs, underscoring the non-uniqueness of the solution and highlighting the spatial (i.e., textural) and temporal (i.e., water content and salinity) variability of soil properties influencing EC at the Pecan_fine_Ivey and Pecan_coarse_Ivey sites.

Among the two sites and dates modeled, the Pecan_fine_Ivey inversion models for 9/6/2023 and 7/16/2022 yield the most representative modeled EC relative to soil sensor EC and serve to validate interpretations that soil texture and water content control electrical conductivity (Figures 19A and 19B). Because soil sensors operate at higher frequencies and sample significantly smaller volumes than EMI instruments, volumetrically homogeneous fine-grained soils are expected to exhibit comparable EC_a responses from soil sensors and EMI instruments. At the 1.2 m depth on 7/16/2022, the VWC is near saturation (0.40 m^3/m^3) while the soil sensor bulk EC and modeled EC are relatively low (~70 mS/m), which suggests that the irrigation event seven days prior elevated the water content, but likely removed residual salts downward via drainage,

and in turn produced low sensor and modeled EC responses (Figure 18B). However, this interpretation does not agree with previously sampled soils at 1.18 m depth, where the composition was reported to be 1% sand, 39% silt, and 61% clay (Ortiz & Jin, 2021), which suggests that the high clay controls soil EC. At the 1.5 m depth on 7/16/2022, the VWC, soil bulk EC and modeled EC are very low (0.04 m^3/m^3, 21.04 mS/m, and 13.10 mS/m, respectively), suggesting the texture at this depth is coarser than what lies above it, and as a result, drains well, and accumulates minimal salts in response to recent irrigations (Figure 18B). This observation agrees with texture samples collected at 1.57 m depth where the soil is 66% sand (Ortiz & Jin 2021).

From July to September, the VWC in the Pecan_fine_Ivey models decrease in each layer, indicating that the soils dry over time in response to less available water, and the soil EC is thereby controlled by water content particularly over soil layers at depths of 0.15 to 0.75 m (Figures 18B and 18A). Between 0.75 and 1.35 m depths, there are significant differences between the VWC and both the modeled and soil sensor bulk EC (Figures 18A and 18B). This divergence highlights the isolation from the layers above the 1.35 m depth to the layers below it, where the modeled EC remains relatively stable over the 14-month period (~510-532 mS/m) from 1.65-3.65 m depth (approaching the groundwater table at approximately ~2-4 m depth). Below 3.65 m on 7/16/2022, the modeled EC decreases by about 85% from the layer above it (Figure 18B). Below 3.65 m on 9/6/2023, the modeled EC decreases by about 37% from the layer above it (Figure 18A). The increase in modeled EC below 3.65 m over time indicates salt loading in the layer between 1.65 and 3.65 m, which then penetrates deeper into the groundwater beneath depths of 3.65 m.

Generally, there are large variations and uncertainties between the modeled EC and soil sensor bulk EC at Pecan_coarse_Ivey between July and September (Figures 19C and 19D). The greater volumetric grain size variation of coarse-grained soils is exhibited in the EC_a response

deviations from the large volume EMI instruments sample versus the small volume soil sensors sample. While the modeled EC increases with depth from 0.0 to 1.5 m on 9/6/2023, there is a reversal in conductivity in the third layer from 0.96 to 1.5 m on 7/16/2022, which is not in accord with soil sensor bulk EC data on this date. This observation does not align with the interpretation that coarse soils drain well in response to an increase in water content, and therefore dictate EC responses (Figures 18C and 18D). The exception to the large uncertainties seen in both Pecan_coarse_Ivey models lies in the third layer (0.96 to 1.5 m) on 9/6/2023, where the small (3.82 mS/m) EC deviation suggests that the modeled data is accurate for that layer, and the soil bulk EC was likely close to 90 mS/m in this layer (Figures 19C and 18C). This is further validated by the point that soil sensors generally overestimate soil sensor bulk EC (Scudiero et al., 2012).

Similar to the trends seen at Pecan_fine_Ivey over the 14-month period, the Pecan_coarse_Ivey model suggests that salt accumulates in the groundwater below 2.65 m depth (Figures 18D and 18C). Considering that the porosity of sand (~30%) contributes minimally to the electrical conductivity, to achieve a threefold increase in EC from 7/16/2022 to 9/6/2023, a sevenfold increase in salt concentration is implied to get to the substantial salt loading from depths of 2.65 meters and below. However, it is important to note that the Pecan_coarse_Ivey model on 7/16/2022 indicates unrealistically low EC values below the 0.96 m depth. Nonetheless, the overall trend of salt transfer downward is evident over time and in response to two seasons of irrigation events.

The modeled EC values for Pecan_fine_Ivey on 7/16/2022 and 9/6/023 closely approximate the soil sensor bulk EC values, albeit slightly higher. This contradicts the fact that the soil EC sensor operates at 60 MHz, whereas the EM38 operates at a 15 kHz frequency. The higher-frequency soil sensor allows charges to be adsorbed to grain surfaces and respond in micron-scale

movements to field conditions, versus the EM38, which induces millimeter-scale charge movements. Due to the EM38's shorter frequency range and longer signal wavelength, the probability for a charge to encounter a barrier should theoretically lower the EC_a, not raise it as the modeled data indicates. In order for the model to fit the trend of the soil sensor bulk EC data, the 2.0 m and half-space layer conductivities needed to be well above 500 mS/m. ECs of this caliber are indicative of salt dissolution, and unlikely to occur below the layers at this site, and more broadly, the Rio Grande Valley.

Section 6: Conclusion

Time series EMI measurements from the 5R and Ivey Pecan Orchards reveal that soil texture plays a dominant role in controlling spatial patterns of EC_a responses. Consistently low EC_a responses with time observed at specific locations along each transect indicate that coarse-textured soils control the EC_a response, while consistently high EC_a responses over time can be attributed to the dominance of fine-textured soils. Soil texture samples from boreholes confirm respective sand- and clay-dominate textures. Consistent drops in EC_a responses spatially show that preferential flow paths redirect water from finer to coarser textured areas.

Dynamic shifts in temporal EC_a responses point to water content being the primary factor controlling EC_a variations over time. EC_a data recorded before the onset of an irrigation season, and following prolonged periods without an irrigation, exhibit the lowest responses over the course of the study. Subsequently, these responses increase post-irrigation, then decrease uniformly over time, with the exception of the 6.0 DOI where EC_a measurements were captured beneath the groundwater table.

The intricate connection between soil texture, water content, and salinity is a key determinant of EC_a responses over time at both sites. Soil texture influences relative water-holding times and salinity, affecting the EC_a response. The observed general increase in EC_a responses with depth is likely caused by the combination of soil water content increases and heterogeneous soil textures. Relatively less saline irrigation water sourced from the Rio Grande throughout the course of the study indicates the role that water content, over salinity, plays in EC_a responses.

While both sites received the same amount and source of irrigation water and show comparable trends in temporal and spatial EC_a responses, it is probable that soils at Ivey are finer

than those at 5R. This finer texture may contribute to the accumulation of water and salts at shallow depths, consequently resulting in higher EC_a responses compared to 5R.

Modeling electrical conductivities on various dates reveal site- and layer-specific electrical conductivities that vary in accuracy, emphasizing permanent and spatial-temporal patterns that soil properties have on EC. On dates when the models were representative of soil sensor EC, interpretations could be made that validate soil texture and water content as controls on EC. At depths below soil sensor locations, modeling alone shows likely salt loading in the groundwater over the 14-month study period.

Factors that were not accounted for in this study, but contribute to the EC_a response include soil temperature, organic matter content, and varying amounts of vegetative cover at the study sites depending on the time of year. Assumptions were made that the EMI instruments were operated "under low induction numbers," (where the secondary field is proportional to the ground current and subsequently used to calculate the EC_a). However, responses at the study sites were relatively high, indicating the possibility that the EC_a responses were not always optimal. The modeled ECs varied in accuracy between time, sites, and depth relative to soil sensor measurements and textural data. This variability introduced challenges to achieving optimal and consistent interpretations.

Future Work

Future research will continue at both pecan orchards in contribution to the NSF-funded Dryland Critical Zone project. The entirety of Ivey Pecan orchard will be surveyed using the EM38 in the VDO (0.75 m DOI) to capture EC_a data previously only surveyed with the EM31. This data will be combined with geochemical, biological, and isotopic data used to monitor the spatial and temporal dynamics of tree size, CO2, salt buildup, crop yield, and soil moisture in agricultural irrigated drylands. Time series EMI data collected at 5R can be compared to soil sensor VWC and bulk EC data at the Pecan_fine_5R and Pecan_coarse_5R locations to better understand spatial and temporal trends and controls on EC_a. Efforts can be made to deconvolve the EC_a response into its constituent components (i.e., salinity, water content, and texture). EMI data from this research will be combined with soil sensor data to facilitate the complex problem of parsing bulk EC into fluid EC and soil moisture.

References

Altdorff, D., Sadatcharam K., Unc, A., Krishnapillai, M., & Galagedara, L. (2020). Comparison of Multi-Frequency and Multi-Coil Electromagnetic Induction (EMI) for Mapping Properties in Shallow Podsolic Soils. *Sensors*, *20*(8), 2330. https://doi.org/10.3390/s20082330

Abudu, S., Sheng, Z., Michelsen, A., & Rodriguez, O., & King, J. (2016, December). *Evapotranspiration and Crop Coefficient for Pecan Trees in El Paso, Texas* [paper presentation]. 2016 Irrigation Show & Education, Las Vegas, Nevada, United States. https://www.researchgate.net/publication/311571352_Evapotranspiration_and_Crop_Coefficient_for_Pecan_Trees_in_El_Paso_Texas

Allred, B., Daniels, J., & Ehsani, M. (2008). *Handbook of agricultural geophysics (Books in Soils, Plants, and the Environment)*. CRC Press. https://doi.org/10.1201/9781420019353

Corwin, D.L., & S.M. Lesch. (2005). Apparent Soil Electrical Conductivity Measurements in Agriculture. Computers and Electronics in Agriculture, 46(1-3), 11–43. https://doi.org/10.1016/j.compag.2004.10.005

De Carlo, L., Vivaldi, G. A., & Caputo, M. C. (2021). Electromagnetic induction measurements for investigating soil salinization caused by saline reclaimed water. *Atmosphere*, *13*(1), 73. https://doi.org/10.3390/atmos13010073

de Jong, E., Ballantyne, A.K., Cameron, D.R. & Read, D.W.L. (1979). Measurement of Apparent Electrical Conductivity of Soils by an Electromagnetic Induction Probe to Aid Salinity Surveys. *Soil Science Society of America Journal*, *43*(4), 810-812. https://doi.org/10.2136/sssaj1979.03615995004300040040x

Doolittle, J. A., & Brevik, E. C. (2014). The use of electromagnetic induction techniques in soils studies. *Geoderma, 223–225*, 33–45. https://doi.org/10.1016/j.geoderma.2014.01.027

Doser, D. I., Dena-Ornelas, O. S., Langford, R. P., & Baker, M. R. (2004). Monitoring yearly changes and their influence on electrical properties of the shallow subsurface at two sites near the Rio Grande, West Texas. *Journal of Environmental and Engineering Geophysics*, *9*(4), 179–190. https://doi.org/10.4133/JEEG9.4.179

Doser, D. I., Ornelas, M. A., Martinez, I., Jin, L., Ortiz, A., & Kaip, G. M. (2019). Using geophysics to investigate texture and salinity of agricultural soils and their impact on crop growth in El Paso county, Texas. *Journal of Environmental and Engineering Geophysics*, *24*(3), 465–477. https://doi.org/10.2113/JEEG24.3.465

Doser, D. I., & Baker, M. R. (2021). Geophysical reconnaissance for siting dryland critical-zone monitoring experiments in southern New Mexico, USA. *Journal of Environmental and Engineering Geophysics*, *26*(4), 255–266. https://doi.org/10.32389/JEEG21-022

Garcia, A. (2021). *Geophysical studies of the characteristics of fluvial and desert soils in Rio Grande valley of west Texas and southern New Mexico.* [M.S. Thesis, The University of Texas at El Paso]. Open Access Theses & Dissertations. https://scholarworks.utep.edu/open_etd/3413

Geonics Limited. (2007). Geonics Limited EM31 SH Manual. ManualsLib. https://www.manualslib.com/manual/2082588/Geonics-Limited-Em31-Sh.html

Geonics Limited. (2016). Geonics Limited EM38 Mk2 Series Manual. ManualsLib. https://www.manualslib.com/manual/1983693/Geonics-Limited-Em38-Mk2-Series.html

Hawley, J. W., Kennedy, J. F., Granados-Olivas, A., & Ortiz, M. A. (2009). *Hydrogeologic Framework of the Binational Western Hueco Bolson-Paseo del Norte Area, Texas, New*

Mexico, and Chihuahua: Overview and Progress Report on Digital-Model Development (No. 349). New Mexico Water Resources Research Institute.

Heil, K., & Schmidhalter, U. (2012). Characterisation of Soil Texture Variability Using the Apparent Soil Electrical Conductivity at a Highly Variable Site. Computers & Geosciences, 39, 98–110. https://doi.org/10.1016/j.cageo.2011.06.017

Hendrickx, J., & Flury, M. (2001). Uniform and Preferential Flow Mechanisms in the Vadose Zone in Conceptual Models of Flow and Transport in the Fractured Vadose Zone. Washington, DC: The National Academies Press. https://doi.org/10.17226/10102

Jaja, N. (2016). Understanding the Texture of Your Soil for Agricultural Productivity. *Virginia Cooperative Extension,* (CSES-162P), 1.

Johnson, C.K., Doran, J.W., Eghball, B., Eigenberg, R.A., Wienhold, B.J., & Woodbury, B.L. (2003, July). Status of soil electrical conductivity studies by central state researchers [paper presentation]. 2023 ASAE Annual International Meeting, Las Vegas, Nevada, United States.

Liu, Y., & Sheng, Z. (2013). soil moisture status in an irrigated pecan field. *Journal of Irrigation and Drainage Engineering*, *139*(1), 26–40. https://doi.org/10.1061/(ASCE)IR.1943-4774.0000503

Luo, Y., Xue, D., & Wang, M. (2010). Reduction to the pole at the geomagnetic equator. *Chinese J. Geophys.*, *53*, 1082-1089. https://doi.org/10.1002/cjg2.1578

Mack, G. H., & Leeder, M. R. (1998). Channel shifting of the Rio Grande, southern Rio Grande rift: Implications for alluvial stratigraphic models. *Sedimentary Geology*, *117*(3–4), 207–219. https://doi.org/10.1016/S0037-0738(98)00015-3

McNeill, J. (1980). *Electromagnetic terrain conductivity measurement at low induction numbers.* Technical Note TN-6. Geonics Limited. http://www.geonics.com/pdfs/technicalnotes/tn6.pdf

Miyamoto, S., Henggeler, J., & Storey, J. B. (1995). Water management in irrigated pecan orchards in the southwestern United States. *HortTechnology*, *5*(3), 214–218. https://doi.org/10.21273/HORTTECH.5.3.214

National Geophysical Data Center (n.d.). International Geomagnetic Reference Field. National Oceanic and Atmospheric Administration (NOAA). https://www.ngdc.noaa.gov/geomag/calculators/magcalc.shtml#igrfwmm

Ortiz, A.C. (2018). *A combined field, experimental and modeling approach to understand the impacts of flood irrigation on pedogenic CaCO3 and CO2 dynamics in drylands*. [Ph.D. Dissertation, The University of Texas at El Paso]. https://scholarworks.utep.edu/open_etd/142

Ortiz, A. C., & Jin, L. (2021). Chemical and hydrological controls on salt accumulation in irrigated soils of southwestern U.S. *Geoderma*, *391*, 114976. https://doi.org/10.1016/j.geoderma.2021.114976

Ortiz, A. C., Jin, L., Ogrinc, N., Kaye, J., Krajnc, B., & Ma, L. (2022). Dryland irrigation increases accumulation rates of pedogenic carbonate and releases soil abiotic CO2. *Scientific Reports*, *12*(1), 464. https://doi.org/10.1038/s41598-021-04226-3

Pathirana, S., Lambot, S., Krishnapillai, M., Cheema, M., Smeaton, C., & Galagedara, L. (2023). Ground-Penetrating Radar and Electromagnetic Induction: Challenges and Opportunities in Agriculture. *Remote Sensing*, *15*(11), 2932. https://doi.org/10.3390/rs15112932

Robinet, J., von Hebel, C., Govers, G., van der Kruk, J., Minella, J. P. G., Schlesner, A., Ameijeiras-Mariño, Y., & Vanderborght, J. (2018). Spatial variability of soil water content and soil electrical conductivity across scales derived from electromagnetic induction and time domain reflectometry. *Geoderma, 314*, 160–174. https://doi.org/10.1016/j.geoderma.2017.10.045

Scudiero, E., Berti, A., Teatini, P., & Morari, F. (2012). Simultaneous Monitoring of Soil Water Content and Salinity with a Low-Cost Capacitance-Resistance Probe. Sensors, 12(12), 17588–17607. MDPI AG. http://dx.doi.org/10.3390/s121217588

Shaner, D. L., Khosla, R., Brodahl, M. K., Buchleiter, G. W., & Farahani, H. J. (2008). How well does zone sampling based on soil electrical conductivity maps represent soil variability? *Agronomy Journal*, *100*(5), 1472–1480. https://doi.org/10.2134/agronj2008.0060

Sheng, Z., & Liu, Y. (2015). Evapotranspiration of flood-irrigated pecans under drought conditions in El Paso, TX. (2015). *2015 ASABE / IA Irrigation Symposium: Emerging Technologies for Sustainable Irrigation - A Tribute to the Career of Terry Howell, Sr. Conference Proceedings*, 1–8. https://doi.org/10.13031/irrig.20152133782

Sosa, E. (2019). *A quantitative assessment of trace metals in subsurface soils and groundwater in agricultural fields of El Paso, Texas*. [M.S. Thesis, The University of Texas at El Paso]. https://digitalcommons.utep.edu/open_etd/2012

United States Department of Agriculture National Resources Conservation Service. (2021). *Web Soil Survey*. https://websoilsurvey.sc.egov.usda.gov/App/WebSoilSurvey.aspx

Wollenhaupt, N. C., Richardson, J. L., Foss, J. E., & Doll, E. C. (1986). A rapid method for estimating weighted soil salinity from apparent soil electrical conductivity measured with

an aboveground electromagnetic induction meter. *Canadian Journal of Soil Science*, *66*(2), 315–321. https://doi.org/10.4141/cjss86-032

Zhao, Y., Peth, S., Hallett, P., Wang, X., Giese, M., Gao, Y. & Horn, R. (2011). Factors controlling the spatial patterns of soil moisture in a grazed semi-arid steppe investigated by multivariate geostatistics. *Ecohydrol.*, 4, 36-48. https://doi.org/10.1002/eco.121

Vita

Kristina Sasser completed her Bachelor of Science degree in Community Health from the University of Maryland, College Park in 2013. In 2019, she pivoted her career from wellness to science when she took geoscience and advanced math courses at Montgomery College. In January 2022, she began her Master of Science program in Geophysics from the University of Texas at El Paso where Dr. Mark Engle was her advisor. During Kristina's time as a graduate student, she was a research assistant with the Dryland Critical Zone Project and a teacher's assistant. She presented at the American Geophysical Union conference in 2022. In summer 2023, Kristina was an intern supporting the National Nuclear Security Administration's Office of Defense Nuclear Nonproliferation. In 2023, she was awarded the Environmental and Engineering Geophysical Society Foundation's 2023 graduate student scholarship and received 1st place for outstanding graduate poster presentation at UTEP's Department of Earth, Environmental and Resource Science's Colloquium.